7

8

9

10

11

13

14

15

17

18 19

20 21

22

23

24

25

26

27

28

29

30

31

32

33

34

35

36

37

38

39

40

41

42

43

44

45





- 1 Response of phytoplankton communities to the onset of the 2020 summer marine heatwave 2 in the Drake Passage and Antarctic Peninsula.
- Andrés S. Rigual-Hernández<sup>1,\*</sup>, Amy Leventer<sup>2</sup>, Manuel Fernández-Barba<sup>3</sup>, José A. Flores<sup>1</sup>, Gabriel Navarro<sup>3</sup>, Johan Etourneau<sup>4</sup>, Dimitris Evangelinos<sup>5,6</sup>, Megan Duffy<sup>2</sup>, Carlota Escutia<sup>7</sup>, Fernando Bohoyo<sup>8</sup>, Manon Sabourdy<sup>4,9</sup> Francisco J. Jiménez-Espejo<sup>7</sup>, and María A. Bárcena<sup>1</sup>
  - Área de Paleontología, Departamento de Geología, Universidad de Salamanca, 37008
    Salamanca, Spain
    - 2. Department of Geology, Colgate University, Hamilton, NY, USA.
  - Department of Ecology and Coastal Management, Institute of Marine Sciences of Andalusia (ICMAN), Spanish National Research Council (CSIC), 11519 Puerto Real, Cádiz, Spain.
- 12 4. University of Bordeaux, CNRS, Bordeaux INP, EPOC, UMR 5805, Pessac, France.
  - GRC Geociències Marines, Departament de Dinàmica de la Terra i de l'Oceà, Universitat de Barcelona, Barcelona, Spain.
  - Department of Earth Science and Engineering, Imperial College London, London, UK.
- 7. Instituto Andaluz de Ciencias de la Tierra (IACT-CSIC), Armilla, Spain.
  - 8. Instituto Geológico y Minero de España (IGME), Madrid, Spain.
  - Laboratoire des Sciences du Climat et de l'Environnement, LSCE/IPSL, UMR CEA-CNRS-UVSQ 8212 CEA Saclay, Gif sur Yvette

\* Corresponding author. E-mail address: arigual@usal.es (A.S. Rigual-Hernández).

# Abstract

Extreme warming events are increasingly more intense and frequent in the global ocean. These events are predicted to drive profound and widespread effects on marine ecosystems, yet their impact on phytoplankton, the base of the marine food web, are still largely unknown. Our understanding of the impact of these phenomena in marine ecosystems is particularly poor in the remote and logistically challenging Southern Ocean. During summer 2020, the research vessel Hespérides sampled the water column of the Drake Passage and northern Antarctic Peninsula before (early January) and during the early phase (late January-early February) of a marine heat wave, that resulted in sea surface temperature anomalies of up to +3°C. Here, we take advantage of this exceptional opportunity to document the effects of an extreme warming event on the nutrient and phytoplankton (diatom and coccolithophores) distributions across the main zonal systems of the Southern Ocean. Overall, our results indicate that biogeographical variability of diatom and coccolithophore assemblages, the two dominant phytoplankton group in the Southern Ocean, mirrored the physical and chemical properties of the water masses delineated by the Southern Ocean fronts. Analysis of a suite of satellite-derived oceanographic parameters revealed that development and persistence of the 2020 marine heat wave were closely tied to mesoscale anticyclonic eddy dynamics. The increase in sea surface temperatures during the onset of the marine heat wave was associated with a remarkable increase in diatom abundance, that reached bloom concentrations, and a shift in the diatom assemblages towards an increase in the relative abundance of the small diatom Fragilariopsis cylindrus/nana in the southern Drake Passage. In turn, coccolithophore abundance decreased north of the polar front during the warm water event, most likely due to a remarkable decrease of nitrate by approximately one order of magnitude lower than average summer concentrations. We speculate that these unusually low nitrate levels were the result of either the advection of nitrate





poor waters from lower latitudes by an anticyclonic eddy and/or nutrient consumption by substantial development of soft-tissue phytoplankton biomass. Overall, our results reinforce the notion that a warmer Southern Ocean will favour an increase of small phytoplankton cells in the southern Drake Passage and northern Antarctic Peninsula with unpredictable consequences in the marine-food web and biogeochemical cycles that need to be urgently quantified and parametrized.

#### 1. Introduction

The global ocean is warming at an unprecedented rapid rate, with modern global sea surface temperatures being nearly 1°C higher than 1850–1900 as a result of anthropogenic climate change (Lee et al., 2023). One consequence of this temperature rise is the increased likelihood of Marine Heat Waves (MHWs; Holbrook et al., 2019) which can be broadly defined as periods of anomalously high warm water temperatures that may last up to several months and may cover thousands of square kilometres (Oliver et al., 2021). These extreme warm ocean temperature events can lead to substantial and diverse impacts on marine ecosystems, such as, (i) global-scale coral bleaching events (Eakin et al., 2019), (ii) profound changes in diversity and structure of marine ecosystems (Wernberg et al., 2013; Wernberg et al., 2016; Garrabou et al., 2022), (iii) reduction of carbon sequestration (Gao et al., 2021), (iv) shifts in the geographical distributions of zooplankton and (v) mass mortalities of mammals and birds (Bond et al., 2015; Cavole et al., 2016; Hobday et al., 2018). However, little information exists about the effects of marine heatwaves on phytoplankton that represent the base of marine food webs and regulate biogeochemical cycles in the ocean (Hayashida et al., 2020).

The Antarctic Peninsula (AP) is one of the fastest warming regions in the world's oceans (Vaughan et al., 2003; Jones et al., 2019; Gorodetskaya et al., 2023) and is experiencing an increase in the frequency of extreme warming events both in the atmosphere (Turner et al., 2021) and in the ocean (Montie et al., 2020). The increase in air and sea surface temperatures are shortening the sea ice season and driving the retreat of glaciers at an increasingly accelerating rate (Cook et al., 2005; Eayrs et al., 2019; Blanchard-Wrigglesworth et al., 2021; Suryawanshi et al., 2023; Davison et al., 2024). The enhanced influx of fresh waters in coastal waters due to ice melting results in a strengthening of the stratification of the water column, while the increase of lithogenic particles - derived from subglacial erosion - increases turbidity and enriches the surface ocean with nutrients (Meredith et al., 2018). The abundance, structure and function of phytoplankton communities in the AP are experiencing changes driven by this rapid environmental change. Primary production has increased in the Western Antarctic Peninsula (WAP) during the last two decades (1998 to 2022), mainly due to the decline in sea ice coverage that results in longer blooms (Ferreira et al., 2024; Isla et al., 2025). As summarized in the comprehensive review by Deppeler and Davidson (2017), changes in the makeup of AP phytoplankton communities could also have profound effects in the local food chain (Ballerini et al., 2014). Freshening of surface waters is expected to drive a shift from diatom-dominated communities to cryptophytes and small flagellates (Moline et al., 2004; Montes-Hugo et al., 2008). Since krill feed mainly of phytoplankton cells larger than 10 μm, the overall size reduction of phytoplankton communities has resulted in a decrease of krill numbers and an increase in salp abundance (grazers unaffected by the size of their prey) (Moline et al., 2004; Moline et al., 2008; Plum et al., 2020; Pauli et al., 2021). Since salps are not a preferred food source for some of the major macrofaunal groups of the AP, such as penguins and seals, changes in the composition of phytoplankton populations towards smaller and non-siliceous phytoplankton are anticipated to have detrimental effects in the whole ecosystem.





Moreover, the climate-induced changes in phytoplankton communities are likely to alter the functioning of biogeochemical cycles in the AP, particularly the carbon cycle through impacts in the biological pump. On the one hand, ice loss results (i) in the fertilization of the surface ocean with nutrients fuelling phytoplankton blooms in areas previously covered by ice and in wake of icebergs (Bertolin and Schloss, 2009; Vernet et al., 2012) and (ii) in the creation of new carbon sinks in open ocean environments (Peck et al., 2010). On the other hand, the abovementioned shift in dominance from diatoms to cryptophytes will most likely result in a less efficient biological pump. This is because the organic content of particles lacking mineral ballast (such as cryptophytes) remineralizes at shallower depths than those associated with biominerals (e.g., opal) and fast-sinking aggregates, such as those formed by diatoms and krill (Green et al., 1998; Smetacek et al., 2004). The net effect of all above mentioned changes over the AP marine ecosystems and their biogeochemical cycles is yet to be determined.

Notably, despite a growing body of evidence that supports the major influence of climate change and its cascading impacts on AP ecosystems (Plum et al., 2020; Oh et al., 2022; Thomalla et al., 2023; Ferreira et al., 2024), very limited scientific studies have addressed the effects of short-term climate extremes (such as MHWs) on phytoplankton primary productivity (Fernández-Barba et al., 2024) and its composition (Antoni et al., 2020). This information is particularly important because of temperature is one of the main factors controlling phytoplankton productivity (Eppley, 1972). One of the few field-based evidence studies addressing this point is the work by Latorre et al. (2023) who documented changes in the biomass of most plankton species in relation to an atmospheric heatwave in a cove of King George Island, South Shetlands. However, the effects of the local scale forcing in this small inlet make the extrapolation of their results to pelagic environments of the AP and Drake Passage difficult. Results of a near-global ocean physical-biogeochemical model indicate that background nutrient conditions most likely represents a major control in determining the impact of heatwaves on phytoplankton productivity (Hayashida et al., 2020). While in nutrient-poor regions marine heatwaves generally will result in weaker phytoplankton blooms, in nutrient-rich waters the heatwave blooms are predicted to result in higher phytoplankton numbers. Based on this notion, phytoplankton growth in the nutrient-rich waters of the AP will be most likely stimulated by marine heatwaves. Since the frequency and intensity of MHWs are expected to substantially increase in the coming decades (Frölicher et al., 2018; Oliver et al., 2018; Oliver et al., 2021), it is of critical importance to evaluate their impacts on Southern Ocean marine ecosystems.

Here we report on data of major phytoplankton groups (diatoms and coccolithophores), and nutrient (silicate, nitrate and phosphate) and environmental parameters (temperature and salinity) collected onboard of the Spanish research vessel Hespérides before and during the onset of a marine heatwave that affected the Drake Passage and AP during January and February 2020. Moreover, we characterize the drivers of the warm water anomaly registered during the northbound transit using satellite-derived and reanalysis data. Our study was partly prompted by previous research (Moline et al., 2004; Montes-Hugo et al., 2008) that indicates that increasing warming in Antarctic ecosystems is causing a change in the abundance, composition and shift from large to small cells of phytoplankton communities. We looked to assess if extreme warming events, that are expected to be more frequent in the coming decades, can also lead to changes in phytoplankton abundance and/or composition. Any shift in phytoplankton community structure and abundance could result in profound changes in the marine food web and biogeochemical cycles, and therefore, they need to be urgently determined and parametrized.



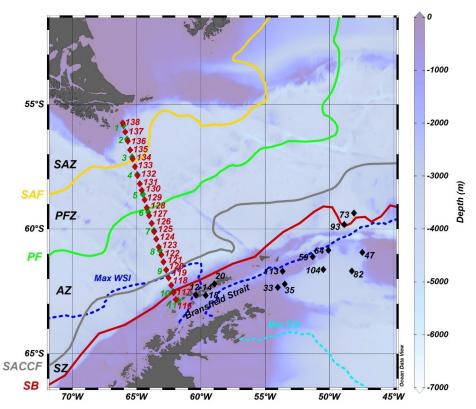


**Figure 1**. Bathymetric map showing the sampling locations during the POWELL-2020 campaing in the Drake Passage and northern Antarctic Peninsula. Green and red diamonds represent stations sampled during the southbound (4<sup>th</sup> to 5<sup>th</sup> of January 2020) and northound (31<sup>st</sup> January to 2<sup>nd</sup> February 2020) transits, respectively, while back dots depict representative stations from the Bransfield Strait and northern Weddell Sea analyzed in this study. Abbreviations: SAZ — Subantarctic Zone, SAF — Subantarctic Front, PFZ — Polar Frontal Zone, PF — polar front, AZ — Antarctic zone, SACCF — Southern e Antarctic Circumpolar Current Front, SZ — Southern Zone and SB — Southern Boundary, Max WSI — maximum winter sea ice extent and Min SSI — minimum summer sea ice extent. Oceanic fronts after Orsi et al. (1995) and sea ice climatology for 1981 to 2010 (Fetterer et al., 2002, updated 2009). Ocean Data View software (Schlitzer, 2021) was used to generate this figure.

### 1.2 Oceanographic setting

The study region covered in the present work is the Drake Passage, the Bransfield Strait and the Powell Basin, extending approximately from 56°S to 64°S and 64°W to 47°W (Fig. 1). The Antarctic Circumpolar Current (ACC), the world's largest ocean current system, flows from west to east in the Drake Passage, connecting surface and deep layers of the ocean (Rintoul et al., 2018). The ACC consists of four major hydrographic fronts from north to south within the Drake Passage: the Subantarctic Zone (SAZ), the Subantarctic Front (SAF), the Southern Antarctic Circumpolar Front (SACCF) and the Southern Boundary front (Orsi et al., 1995; Rintoul et al.,





2018). The Drake Passage is the narrowest constriction of the Antarctic Circumpolar Current (ACC), with a width of approximately 800 km. As a result, the ACC fronts are closely spaced in this region compared to other sectors of the Southern Ocean (Meredith et al., 2011). The position of the above-mentioned fronts exhibit temporal variations and are influenced by disturbances by mesoscale eddies and meanders (e.g. Rintoul et al., 1997; Rintoul and Sokolov, 2001). Both models and observations indicate the Drake Passage is one of the few key areas in the Southern Ocean where eddy heat transport across the ACC fronts is intensified (e.g. Gutierrez-Villanueva et al., 2020).

Phytoplankton growth in the Southern Ocean is controlled by multiple environmental factors, among which low light levels in deep wind-mixed surface layers and low concentrations of the micronutrient iron, stand out as the main factors controlling primary production (Martin et al., 1990; Boyd and Trull, 2007; Venables and Moore, 2010). The ACC carries Circumpolar Deep Water (CDW), the most widespread water mass in the Southern Ocean. Wind-driven upwelling of CDW south of the PF brings to the surface layer large amounts of nutrients and CO<sub>2</sub> (Toggweiler and Samuels, 1995) that fuel primary productivity. However, the biological uptake of these nutrients is far from complete, with much of the Southern Ocean containing high nutrient concentrations and low phytoplankton biomass. These conditions make the Southern Ocean the largest high-nutrient, low chlorophyll (HNLC) region in the world ocean. The surface waters of the Drake Passage and of the mid- to outer-shelf of the AP are severely iron limited (< 0.1 nmol kg-1; Klunder et al., 2014; Annett et al., 2017) thereby restricting phytoplankton growth. In turn, in the Bransfield Strait and coastal systems of the AP, re-suspension of iron-rich sediments and melting of glaciers result in generally iron replete waters that support high primary production (Ardelan et al., 2010).

### 2. Material and methods

# 2.1. The POWELL-2020 campaign

The POWELL-2020 campaign took place onboard the *R/V Hespérides* from 2 January to 4 February 2020. During the POWELL2020 campaign, 150 stations were sampled during the crossing of the Drake Passage, in the Bransfield Strait, and in the Powell Basin. In these areas, seawater samples were collected from the ship's continuous intake at 5 meters depth. During the southbound transit, surface seawater samples were collected every 3–4 hours to capture key changes across the different ACC fronts. On the return (northbound) transit, sampling was conducted every 2 hours. Within the Bransfield Strait and Powell Basin, sampling intervals were generally every approximately 4 hours, adjusted according to other ongoing research activities.

Three types of filters were used: the 0.45-micron HAWG filter for diatoms, coccolithophores, and dinoflagellates; the 0.45-micron HAWP filter for other organisms; and GFF filters for pigments, suspended material, and carbon/nitrogen isotopes. Pigments, C/N isotopes, and HAWP filters were stored in aluminum foil and Petri dishes at -80°C, following rapid freezing with liquid nitrogen. The filters for phytoplankton were stored at room temperature in Petri dishes and left to dry for two days.

### 2.2. Satellite-derived and reanalysis data

European Space Agency (ESA) Climate Change Initiative (CCI) and Copernicus Climate Change Service (C3S) SST data spanning from 1982 to 2021 (Merchant et al., 2019; https://doi.org/10.48670/moi-00169; last accessed: May 2025) was used to analyze warm water anomalies. This satellite-derived, reprocessed Level 4 (L4) product provides global, gap-free daily SST at a 0.05° × 0.05° horizontal resolution, allowing for a comprehensive spatiotemporal

206

207208

209

210

211

212

213

214

215

216

217

218 219

220

221

222

223

224

225

226

227

228

229

230

231

232

233

234

235

236

237

238

239

240

241

242

243

244

246

247

248





characterization of MHWs worldwide (e.g. Martínez et al., 2023; Bell et al., 2024; Fernández-Barba et al., 2024). MHWs were then identified based on the methodology outlined by Hobday et al. (2016) and Oliver et al. (2021), with the additional criterion of the long-term mean summer temperature (LMST), as described by Fernández-Barba et al. (2024). Specifically: (i) SSTs must exceed the seasonally varying 95th percentile (relative to 1982-2012), (ii) for a minimum duration of 5 consecutive days, (iii) with gaps of less than 3 days, and (iv) the mean SST must be higher than the LMST. The rationale for including this additional criterion was to exclude winter MHW events, thereby retaining only those that occurred during the austral summer, the season during which the POWELL-2020 campaign took place. As discrete yet prolonged events, MHWs occurred over defined periods during which SST exceeded a specified threshold (the 95th percentile in this work). Therefore, MHW events were spatiotemporal characterized using metrics widely applied in previous studies (see Oliver et al., 2018; Oliver et al., 2021). In our study, MHW duration was calculated as the time interval (in days) between the onset and the end of each event. Since more than one event may occur within a given year, we also calculated total annual MHW days, defined as the sum of all days in a year during which SST exceeded the MHW threshold. Maximum intensities of MHWs were also calculated as the greatest difference between the absolute temperature and the seasonally varying threshold during each event. Based on this metric, MHW events were categorized according to the number of times the maximum intensity exceeded the difference between the climatological mean and the 95thpercentile threshold (Hobday et al., 2018; Oliver et al., 2021). Thus, events were classified from category 1 to 4 as moderate, strong, severe, and/or extreme, respectively. Additionally, to assess the strength of each event, MHW cumulative intensity was calculated by integrating the event's intensity over its duration. This metric is particularly relevant for evaluating the biogeochemical impacts resulting from MHWs (Oliver et al., 2021; Smith et al., 2023). The general Python code used to detect MHWs is publicly accessible at <a href="https://github.com/ecjoliver/marineHeatWaves">https://github.com/ecjoliver/marineHeatWaves</a>. adapted code for the Southern Ocean https://github.com/ManuFBarba/Southern-Ocean-MHWs.

To assess the influence of regional ocean dynamics, particularly mesoscale eddies, on the development of the 2020 MHW in the Drake Passage, satellite altimetry-derived variables from the Copernicus Marine Service (CMS) Global Ocean Gridded L4 Sea Surface Heights and Derived Variables product were analyzed. This dataset merges Level 3 along-track altimetric observations from multiple satellite missions into a global gridded product with a spatial resolution of 0.125° × 0.125° (https://doi.org/10.48670/moi-00148; last accessed: May 2025). Specifically, sea level anomaly (SLA) and absolute dynamic topography (ADT) were obtained for the period 1993–2021. These variables provide a first-order approximation of mesoscale circulation patterns modulating the upper-ocean thermal structure. Positive SLA values are typically associated with warmer surface conditions, while negative anomalies generally indicate cooler waters, reflecting the thermal imprint of eddy-driven dynamics (Beech et al., 2022; He et al., 2024). SLA was derived relative to a 20-year mean dynamic topography (MDT) baseline (1993–2012), following the equation:

245 SLA = SSH – MDT

Where SSH is the instantaneous sea surface height, and MDT represents the long-term mean difference between sea level and the geoid (equipotential surface). Then, ADT corresponds to the absolute sea surface height referenced to the geoid, given by:

249 ADT = SLA + MDT





250 ADT is directly related to the geostrophic surface velocity field. The zonal  $(u_g)$  and 251 meridional ( $v_{\rm g}$ ) components of geostrophic velocity were computed as:

- Where g is the gravitational acceleration, f is the Coriolis parameter (f =  $2\Omega \sin \phi$ ;  $\phi$  = latitude). 254
- 255 Then, to further characterize mesoscale activity, Eddy Kinetic Energy (EKE) was computed from
- 256 geostrophic velocity anomalies.

257 
$$EKE = \frac{1}{2} \left( u_g^{\prime 2} + v_g^{\prime 2} \right)$$

- Where  $u_g'=u_g-\langle u_g\rangle$  and  $v_g'=v_g-\langle v_g\rangle$  represent the deviations from the long-term mean 258
- geostrophic velocities ( $\langle u_a \rangle$  and  $\langle v_a \rangle$ , respectively). Moreover, to quantify kinetic energy 259
- redistribution throughout the water column, Vertically-Integrated Kinetic Energy (VIKE) was 260
- 261 computed as:

263

264 265

266

267

268

269

270

271

272

273

274

275

276

277

278

279

280

281

282

283

284

285 286

287

262 
$$VIKE = \int_{z_1}^{z_2} \frac{1}{2} \rho(u^2 + v^2 + w^2) dz$$

Where  $\rho$  is the seawater density profile, obtained from the CMS Global Ocean Physics Reanalysis (https://doi.org/10.48670/moi-00021; last accessed: May 2025) at 0.083° x 0.083° horizontal resolution, and u, v, and w are the three-dimensional velocity components. VIKE is a critical diagnostic to quantify the contribution of mesoscale eddies to the vertical energy structure of the ocean and their potential role in modulating SST and triggering MHWs (Bian et al., 2023).

To investigate the atmospheric drivers, radiative fluxes, and surface energy inputs contributing to the onset of the 2020 MHW in the Drake Passage, key variables from the European Centre for Medium-Range Weather Forecasts (ECMWF) ERA5 reanalysis product, provided by the C3S (Hersbach et al., 2023; https://doi.org/10.24381/cds.adbb2d47; last accessed: May 2025) were analyzed. This global reanalysis combines model outputs with observational data to generate a product at 0.25° x 0.25° horizontal resolution, which has been extensively validated in the Southern Ocean and has outperformed other reanalyses (Gossart et al., 2019; Tetzner et al., 2019; Zhu et al., 2021). Specifically, anomalies of variables directly linked to heat transfer (2m-Air temperature and 10m-Wind Speed), radiative forcing (Surface net shortwave radiation flux, Surface net long-wave radiation flux, Surface downward short-wave radiation flux, and Surface downward long-wave radiation flux), and surface sea-air dynamics (Mean sea level pressure, Surface latent heat flux, Surface sensible heat flux, Turbulent surface stress, and Normalized energy flux into ocean) were calculated relative to a 31-year reference period (1982-2012).

To support our in-situ data, satellite-derived chlorophyll-a (chl-a) data were obtained from the Copernicus Global Ocean Colour (GlobColour) product (https://doi.org/10.48670/moi-00281; last accessed: May 2025). This interpolated L4, multi-satellite product provides daily data at a spatial resolution of 4 km. To enable comparison with in-situ observations and to reinforce the interpretation of local variability, monthly modeled surface dissolved iron concentration from the Global Ocean Biogeochemistry Hindcast dataset





(https://doi.org/10.48670/moi-00019; last accessed: May 2025), at 0.25°×0.25° horizontal resolution was also incorporated.

### 2.3 Nutrient analysis

During the POWELL-2020 campaign, samples were collected in the Drake Passage and the Bransfield Strait, spanning transects between 65°W and 60°W and from 55°S to 63°S (Figure 2). Discrete surface water samples were collected at a depth of approximately 5 meters depth using the underway seawater system. The sampling effort included 140 surface stations distributed approximately every 60 km along the cruise track. Only nutrient data for the 51 stations used for phytoplankton analysis (see section 2.4) are presented here. All samples intended for nutrient analyses were filtered immediately onboard through Whatman polycarbonate membrane filters (0.45  $\mu m$  pore size, 47 mm diameter) to remove particulate material. The filtered samples were frozen at -20°C in 50ml polyethylene vials for N and P nutrients, while they were stored at room temperature for Si measurements. Nutrient concentrations were analysed at UMR EPOC, University of Bordeaux, and measured using two segmented flow autoanalyzer's from Seal Analytical: the AA3HR macroflow analyser was used for the determination of silicates and phosphates, while the quAAtro microflow analyser was used for the determination of nitrites, nitrates, and ammonium, following the protocol of Bendschneider and Robinson (1952) optimized by Aminot et al. (2009). Silicate determination was based on the formation of a silico-molybdate complex, which is reduced by ascorbic acid to form molybdenum blue. Potential interferences from phosphates were eliminated by adding oxalic acid.

Absorbance for silicates was measured at 820 nm. Phosphate detection was established on the fact that phosphates form a phospho-molybdate complex in the presence of antimony, which is reduced by ascorbic acid to produce an intense blue colour. Absorbance was measured at 880 nm. In comparison, nitrites react under acidic conditions with sulphanilamide and N-naphthyl-ethylenediamine (NED) to form a coloured azo dye. Absorbance was then measured at 540 nm. In parallel, nitrates are quantitatively reduced to nitrites using a cadmium-copper reduction column. The resulting nitrites are then measured using the same colorimetric method as for direct nitrite analysis with an absorbance at 550 nm.

### 2.4 Phytoplankton analysis

Discrete samples were collected from the prefiltered and uncontaminated seawater line taken under the ship at 5 m water depth, in one L Nalgene bottles, and filtered immediately through 0.45-micron pore size, 25 mm diameter HAWG gridded mixed cellulose ester membrane filters. Here we present results from 51 stations representative of the main environments sampled during the POWELL-2020 survey. Filters were placed in polystyrene petri dishes and allowed to dry (24-48 hours). Filters were then cut in half, with one half mounted on a glass slide using immersion oil and covered with a cover slip. These slides were used for quantitative analysis of micro- and nannoplankton abundance and assemblage composition using light microscopy at 1000x magnification for diatoms and a microscope equipped with both linear and circular polarization at 1000x for coccolithophore identification. The other half of each filter was stored in the petri dish for Back Scattered Electron Imagery analysis using a Hitachi TM4000 Plus SEM. SEM work of selected samples was conducted to clarify identification of smaller specimens.

In regard to the taxonomic identification of diatoms, each diatom cell (i.e. frustule) was identified to the lowest taxonomic level possible using the taxonomic concepts of Hasle and Syvertsen (1997) and Scott and Marchant (2005). Morphological and molecular analyses by

334

335

336

337

338

339

340

341

342

343

344 345

346

347

348

349

350

351

353

354

355

356

357

358

359

360

361

362

363

364

365

366

367

368

369

370

371

372

373

374

375

376

377





Lundholm and Hasle (2008) revealed that Fragilariopsis cylindrus and Fragilariopsis nana are different species but often they share many morphological characteristics that make their differentiation impossible with light microscopy. Therefore, we followed the approach of Cefarelli et al. (2010) lumping the cell counts of these two species under the name F. cylindrus/nana. In regard to the genus Chaetoceros, three groups were distinguished. The vegetative cells of Chaetoceros subgenus Phaeoceros (which includes C. aequatorialis, C. atlanticus, C. criophilus, C. peruvianus, C. dichaeta, C. pendulus, and C. bulbosum) and Hyalochaete were separated owing to their different habitats (oceanic and neritic, respectively). The resting spores of genus Chaetoceros were identified only to group level due to a lack of morphological criteria. In regard to coccolithophore identification, the taxonomic concepts of Young et al. (2003) and Nannotax website (Young et al., 2024) were followed. The lower coccolithophore diversity observed in our study compared to previous work in the study region (e.g. Charalampopoulou et al., 2016) is attributed to methodology applied. Previous studies used Scanning Electron Microscopy that allow for a more precise identification of coccolithophore species as well as identification of different Emiliania huxleyi and Calcidiscus leptoporus morphotypes. In turn, although light microscopy applied in HAWG filters allows a reliable quantification of coccospheres and characterization of most coccolithophore taxa to genus level, it precluded the identification to species and morphotypes level (e.g. clasification of E. huxleyi or C. leptoporus morphotypes).

#### 352 3. Results

### 3.1 Satellite-derived and model data

### 3.1 Characterization of the marine water anomaly

In late austral summer of 2020, significant MHWs developed in the Drake Passage, closely associated with the presence and dynamics of mesoscale anticyclonic eddies that appear to have contributed to the surface trapping of anomalously warm water masses (Fig. 2). The sea level anomaly (SLA) field, referenced against the 1993-2012 climatology, revealed a distinct positive anomaly pattern along the path of the POWELL-2020 northbound transect (January 31-February 2), with values exceeding +20 cm (Fig. 2a). This elevated SLA, along with heightened Absolute Dynamic Topography (ADT), indicated the likely presence of an eddy-induced elevation in SSH. In fact, the distribution of Eddy Kinetic Energy (EKE) anomalies and the configuration of geostrophic surface currents further supported the interpretation of energetic anticyclonic structures influencing the thermal signature in this highly dynamic region (Fig. 2b). The MHW's thermal impact was considerable. Its peak intensity reached approximately +3°C above climatological thresholds (Fig. 2c), placing it within the moderate to severe category according to the Hobday et al. (2018) classification. It lasted for over 90 days in parts of the Drake Passage (Fig. 2d), with cumulative intensities exceeding, on average, 60°C·days (Fig. 2e), highlighting its strength. Temporal averages along the POWELL-2020 return transect reveal that SLA and ADT anomalies peaked during MHWs periods, consistent with the eddy-driven elevation of SSH (Fig. 2f). Elevated EKE values, considering summertime, during MHWs further suggested intensified mesoscale activity sustaining the events. In contrast, vertically-integrated kinetic energy (VIKE) remained relatively low during MHWs' peaks and rose only after its decline, pointing to a process confined predominantly to the upper ocean. This temporal decoupling supports the interpretation of a surface-intensified phenomenon, later followed by subsurface baroclinic adjustments (Fig. 2f). Overall, these results indicate the important role of ocean-internal dynamics in modulating MHWs in the Drake Passage.



379

380

381

382

383

384

385

386

387

388

389

390

391

392

393

394

395

396

397

398

399

400

401

402

403



To assess the possible atmospheric contribution to these events, near-surface air temperature anomalies, 10-meter wind speeds, and surface heat flux components (shortwave, longwave, latent, and sensible) were also analyzed over the core MHW periods (Supplementary Fig. 1). While January 31-February 2, 2020, was characterized by slightly elevated atmospheric temperatures (Supplementary Fig. 1a), reduced wind speeds in the Drake Passage (Supplementary Fig. 1b), as well as transient increases in radiative and thermal fluxes to the ocean compared to the 1982-2012 period (Supplementary Fig. 1c-h), the net surface heat exchange exhibited a predominantly negative signature during the onset of MHWs (Supplementary Fig. 1i). Notably, the ocean lost energy to the atmosphere in the Drake Passage (Supplementary Fig. 2) through negative net long-wave and latent heat fluxes, despite moderate positive sensible heat contributions (Supplementary Fig. 1i). The relative constancy of windinduced turbulent stress during the MHW onset, with a marked increase only after the event subsided (Supplementary Fig. 1i), suggests that the MHW likely altered local atmospheric dynamics, rather than being driven by them. These results suggest that, while atmospheric anomalies were present and may have facilitated the persistence of the 2020 events, they were insufficient to solely explain the build-up of heat.

Altogether, and considering the occurrence of distinct MHW events throughout the austral summer of 2020, the evidence converges on the conclusion that the 2020 MHWs in the Drake Passage were primarily modulated by isolated anticyclonic eddies. These eddies enhanced stratification, suppressed vertical mixing, and prolonged the retention of warm surface waters, thereby amplifying and sustaining the MHW signal well beyond what would be expected from atmospheric forcing alone (Beech et al., 2022; He et al., 2024).

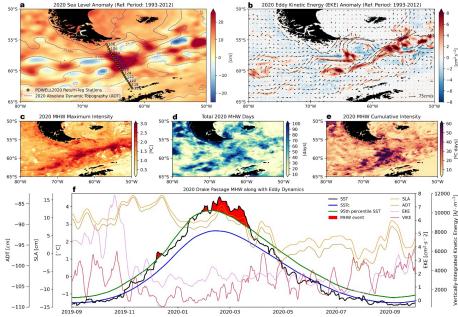


Fig. 2. Characterization of the marine thermal anomaly during the austral summer of 2020 in the Drake Passage. (a) Sea level anomalies (SLA; shading) and absolute dynamic topography (ADT; purple contours), averaged over January 31–February 2, coinciding with the return transect of the POWELL-2020 campaign. (b) Eddy kinetic energy (EKE; shading)





anomalies and surface geostrophic currents (black arrows) from CMS multi-satellite observations. (c-e) Marine heatwave (MHW) properties during the austral summer of 2020, based on ESA CCI C3S L4 sea surface temperature (SST) using the 95th percentile criterion: (c) maximum intensity, (d) total days, and (e) cumulative intensity. (f) Temporal evolution of SLA (orange), ADT (olive), EKE (pink), and Vertically-Integrated Kinetic Energy (VIKE, dark red), together with MHW events (red shading), as indicated by ESA CCI C3S L4 daily SST (black), climatological SST (SSTc, blue), and MHW criterion (95th percentile SST, green), during 2019–2020. Time series represent spatial averages over the return-leg stations of the POWELL-2020 campaign (green dots in (a)). A 7-day running mean filter is applied to EKE and VIKE. The reference period for the SLA and EKE anomalies is 1993–2012 (a, b, and f), while that for MHWs is 1982–2012 (c-f).

#### 3.3 Nutrient distributions

Nutrient distributions in the surface layer across the Drake Passage and Bransfield Strait during January and early February 2020 are illustrated in Figure 3b and summarized in Table 1. During the southbound transit to the Shetland archipelago in early January 2020, nitrate concentration in the subantarctic and polar frontal zone waters ranged between 7.6 and 14.3 and between 9.0 and 17.2 μmol L-1, respectively, while phosphate concentrations ranged between 0.6 and 1.1 and between 1.3 to 1.4 µmol L-1, respectively. Silicate concentration was low in the subantarctic zone (ranging between 2.2 to 2.8) and in most of the PFZ in most of the PFZ with values ranging 1.3 to 2.1 μmol L<sup>-1</sup> except for station 6 were values dramatically increased due to the vicinity of the Polar Front. South of the Polar Front, nitrate and phosphate levels showed a slight increase (13.0 to 17.4 and 1.4 to 1.7 μmol L<sup>-1</sup>, respectively), whilst roughly a tenfold rise in silicate concentrations (17.6-21.6 µmol L-1) was observed. This sharp silicate gradient at the PF is also known as the Silicate Front and represents a critical boundary for nutrient distributions in the Southern Ocean (Freeman et al., 2019; Table 1). South of the SB and in the Bransfield Strait, nitrate and phosphate levels exhibit concentrations similar to those documented in the AZ waters (Fig. 3b). In turn, silicate concentrations exhibited the highest levels of the meridional gradient, with values up to 77.0 μmol L<sup>-1</sup> (Fig. 3b).

During the northbound transit in late-January early-February, the main biogeochemical Southern Ocean zones remained clearly evidenced in the nutrient distributions. However, some important differences compared with the southbound transit were noticed. Nitrate and phosphate levels north of the PF decreased about one order of magnitude (down to 0.8 and 0.6  $\mu$ mol L<sup>-1</sup>, respectively) compared to those registered in the southbound transit. In contrast, the meridional distribution of silicate remained similar to that documented in the southbound transit (Fig. 3b).





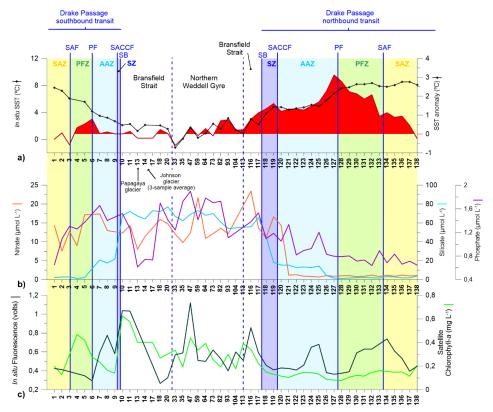


**Figure 3.** a) SSTs and SST anomaly. b) nutrient concentrations (nitrate, silicate and phosphate). c) Fluorescence (*in situ*) and satellite chlorophyll-*a* concentration.

**Table 1.** Physical and chemical parameters of the Drake Passage. Interannual average values represent the median and first and third quartiles (between brackets) for silicate, nitrate, phosphate, temperature and salinity between 2004 and 2017 from Freeman et al. (2019) and for Mixed Layer Depth (MLD) between 2004 and 2011 from Stephenson et al. (2012). Variability range of each parameter during the outbound (early January 2020) and northbound transits (Late-January early-February 2020) of the Powell-2020 campaign. \*Freeman et al. (2019) and Stephenson et al. (2012) do not cover the Bransfield Strait but data from this region is presented for the POWELL-2020 campaign.

Zonal system	Time interval	Silicate (µmol/kg)	Nitrate (µmol/kg)	Phosphate (µmol/kg)	Temperature (°C)	Salinity (psu)	MLD (m)	Stations
SAZ	Interannual average	4.6 (3.0-6.5)	20.6 (19.0-21.4)	1.5 (1.4-1.5)	5.6 (5.0-6.0)	34.1 (34.0-34.1)	141.4 (87.1-225.8)	-
	Early January 2020	2.16-2.82	7.6-14.3	0.65-1.30	6.06-7.67	33-33.6	-	1-3
	Late-January early-February 2020	1.77-3.76	0.87-1.17	0.65-0.83	7.8-8.54	33.10-34.60	-	134-138
PFZ	Interannual average	6.7 (4.1-9.8)	22.8 (21.5-24.2)	1.6 (1.5-1.7)	4.5 (3.8-5.3)	34 (34.0-34.1)	82.7 (44.6-144.4)	-
	Early January 2020	1.28-11.68	8.98-17.16	1.26-1.37	4.16-5.57	33.5	-	4-6
	Late-January early-February 2020	1.6-2.2	0.77-1.2	0.64-0.89	7.6-8.35	33.4-34.8	-	128-133
AAZ	Interannual average	21.6 (16.0-29.6)	25.7 (24.7-26.8)	1.7 (1.7-1.8)	0.7 (-0.7-1.9)	33.8 (33.7-33.9)	70.7 (48.3-99.4)	-
	Early January 2020	17.54-21.6	12.97-17.37	1.4-1.66	2.68-3.48	33-33.1	-	7-9
	Late-January early-February 2020	1.7-15.4	0.68-14.36	0.8-1.33	4.40-6.8	33-33.8	-	120-127
SZ - Bransfield Strait*	Interannual average	40.5 (27.4-52.3)	26.3 (23.9-27.8)	1.8 (1.7-2.0)	-0.5 (-1.3-1.0)	33.9 (33.8-34.0)	75 (58.3-96.4)	-
	Early January 2020	64.28-76.96	8.04-15.93	0.61-1.70	1.25-2.28	24.7-33.9	-	10-20
	Late-January early-February 2020	18.14-65.48	11.02-23.43	1.09-1.53	2.2-4.8	33.2-33.5	-	116-119





### 3.3 Phytoplankton abundance variability

In-situ fluorescence measurements at 5 m depth from the ship and satellite-derived Chlorophyll-a (Fig. 3c) followed roughly similar trends (Spearman's correlation coefficient (p) = 0.35, p < 0.05, n = 45). Both parameters indicate maximum algal biomass accumulation in the western Bransfield Strait (in both the southbound and northbound transits) and in the Weddell Sea (Fig. 3). In terms of temporal variability in the Drake Passage (i.e. before and during the onset of the MHW), both average fluorescence and satellite-derived chlorophyll-a in this region suggest relatively similar algal biomass accumulation in the southbound and northbound transits (average fluorescence of 0.49 and 0.52 volts in the southbound and northbound transits, respectively, and average chlorophyll-a concentration of 0.26 and 0.22 mg L<sup>-1</sup>; Fig. 3).

In terms of diatom distributions, total diatom abundance ranged between 0.003 and 5.5 x  $10^6$  cells L<sup>-1</sup> and exhibited a clear increase south of the PF (Fig. 4a). In terms of temporal distribution, diatom abundance within the same zonal systems was generally lower during early January than in late-January and early-February. While there is no universally fixed threshold for what constitutes a phytoplankton bloom, a frequent definition is a proliferation event with cell concentrations reaching or exceeding one million cells per Liter (e.g. Johnsen et al., 1999). Based on this definition, diatom bloom concentrations during the POWELL-2020 campaign were reached during the second half of the expedition in one station in the Bransfield Strait (station 82; Fig. 4a) and, almost consistently, during the northbound transit in the Southern Zone and Antarctic Zone (stations 118-126; Fig. 4a), with cell numbers reaching values up to ca. 5.5 x  $10^6$  and  $5 \times 10^6$  cells L<sup>-1</sup>, respectively.

Coccolithophore abundance was low compared to diatoms, with cell concentrations ranging between 0 and 8 x  $10^4$  coccospheres L<sup>-1</sup> (Fig. 5). Our results reveal a nearly opposite latitudinal distribution than that of the diatoms, with maximum concentrations in the SAZ and PFZ. Coccolithophore abundance was negligible in the Bransfield Strait and northern Weddell Sea, with no coccospheres documented during our counts although a few coccospheres where identified (but not quantified) during SEM analyses. In regard to temporal variability, average coccolithophore abundance in the SAZ and PFZ was two-fold during the southbound transit in early January (3.9 x  $10^4$  coccospheres L<sup>-1</sup>) than during the northbound transit in late January-early February (ca.  $1.8 \times 10^4$  coccospheres L<sup>-1</sup>). Coccolithophore assemblages were composed of two species: *E. huxleyi* and *C. leptoporus*.





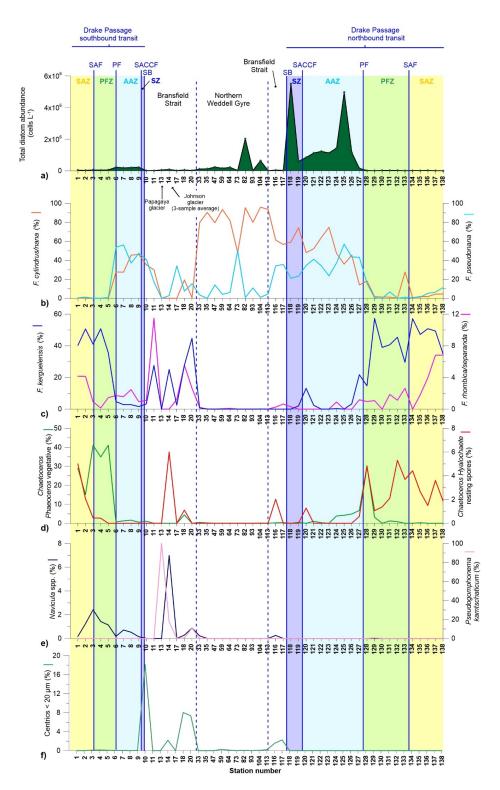






**Figure 4.** a) Diatom cell concentration in the upper layer (5 m depth) documented in the Drake Passage, Bransfield Strait and Northern Weddell Sea Gyre documented in representative stations of main environments during the POWELL-2020 campaign. b-e) Relative abundance of the most abundant and/or key diatom species.

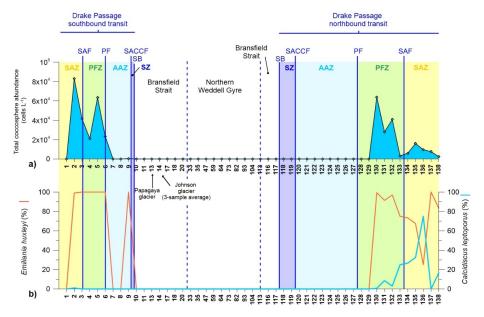


**Figure 5.** a) Coccosphere cell concentration in the upper layer (5 m depth) documented in the Drake Passage, Bransfield Strait and Northern Weddell Sea Gyre documented in representative stations of main environments during the POWELL-2020 campaign. b) Relative abundance of the *Emiliania huxleyi* and *Calcidiscus leptoporus*.

# 3.4 Distribution of phytoplankton species

Fragilariopsis kerguelensis dominated the diatom assemblages in the SAZ and PF (i.e. north of the PF) in both the southbound and northbound transits, with an average contribution of 44 and 42 %, respectively. South of the polar front, *F. kerguelensis* also exhibited relatively high concentrations some stations of the western Bransfield Strait during early summer (up to 45% in station 20; Fig. 4c). Fragilariopsis cylindrus/nana and Fragilariopsis pseudonana displayed a nearly opposite pattern to that of *F. kerguelensis*, dominating the diatom assemblages in most of the stations south the PF. Fragilariopsis cylindrus/nana contributed an average of 52% to the diatom assemblage in all the stations south of the PF, reaching maximum abundances in the northern Weddell Sea stations where its contribution accounted for up 96% of the total diatom assemblage (station 104; Fig. 3). *F. pseudonana* contributed on average 25% of the diatom assemblage south of the PF, with peak contributions in the Antarctic Zone. In terms of temporal variability, some important differences between the southbound and northbound transits were noticed. While *F. cylindrus/nana* represented an average of 37% of the diatom assemblage from the PF southwards in the Drake Passage (i.e. AAZ and SZ) in early January 2020 (i.e. the southbound transit), the relative abundance of this taxon increased to 52% in the same zonal





systems (Fig. 3b). In turn, *F. pseudonana* exhibited a decrease in its relative contribution reaching an average relative contribution in the AAZ and SZ between the southbound (49%) and the northbound transit (36%).

Chaetoceros subgenus Phaeoceros was a major component of the diatom in the SAZ and PFZ (up to 41% of the total diatom assemblage in station 3; Fig. 3d) during the southbound transit. In turn, this taxon only exhibited elevated numbers at one station during the northbound transit (station 127 with a contribution of 30%). The vegetative cells of Chaetoceros subgenus Hyalochaete were only documented in abundances over 1% in the first two stations of the SAZ (stations 1 and 2, with 6 and 2%, respectively; data not shown). Chaetoceros resting spores showed a contrasting distribution in the Drake Passage between the southbound and northbound transits. During the southbound transit, they were only present in the SAZ (up to 5%; Fig. 3d), while during the northbound transit they were consistently documented between the AAZ and SAZ (ranging between 1 and 5%). Chaetoceros resting spores were also present in some stations in the Bransfield Strait (up to 6% in Livingston Island). Notably, the diatom assemblages collected near Papagaya and Johnson glaciers in the coastal waters of Livingston Island (stations 13 and 14) were remarkably different from the rest of the stations and rich in fine sediments. These samples exhibited high abundances of Pseudogomphonema kamtschaticum (average of 38%) and secondary contributions of Navicula spp. (5%). Lastly, the small centric group (that encompasses all small centric diatoms under 20 µm that were not identified to lower taxonomic level) exhibit peak values south of the SB and in the Bransfield Strait in early January, reaching values up to 18% in station 10. Interestingly, SEM imagery revealed that some of the small centrics were Minidiscus chilensis, although it was not possible to quantify its contribution due to the limitations of light microscopy.

Emiliania huxleyi largely dominated the coccolithophore assemblages during our survey with an average relative abundance of ca. 80% in all samples. In regard to temporal variability of coccolithophores, a contrasting distribution of *C. leptoporus* could be observed between the southbound and northbound transits. *C. leptoporus* contribution was negligible during the southbound transit but increased substantially during the northbound transit, reaching values up to 75% of the coccolithophore assemblage in the SAZ (station 136; fig. 5).

### 4. DISCUSION

## 4.1 Characterization of the marine water anomaly

The 2020 MHW observed across the Drake Passage and Antarctic Peninsula (AP) offers valuable insight into the nuanced interplay between mesoscale ocean circulation and biogeochemical variability in the Southern Ocean. Our data reveal that this extreme event was neither solely a product of atmospheric forcing nor simply a reflection of long-term warming trends. Instead, the development and persistence of the 2020 MHW were closely tied to mesoscale anticyclonic eddy dynamics, as indicated by sustained positive SLA exceeding +20 cm along the northbound transect (Fig. 2a). This pattern is characteristic of the Drake Passage, where the proximity of major circumpolar fronts enhances eddy activity relative to other sectors of the Southern Ocean (Rintoul et al., 1997; Beech et al., 2022), resulting in pronounced horizontal and vertical gradients in water properties.

The warm water anomaly recorded during the northbound transit of the POWELL-2020 campaign—immediately preceding the core of the heatwave—coincided with elevated SLA and increased ADT, classic markers of surface-intensified anticyclonic eddies. These features





effectively trap heat, suppressing vertical mixing and allowing anomalously warm, stratified surface waters to persist. Our estimates of EKE and VIKE further support that these events were primarily confined to the upper ocean, with deeper kinetic energy redistribution occurring only after the MHW's peak (Fig. 2f). Satellite-derived SST anomalies revealed sustained surface warming of more than +3°C above climatological values, underscoring the spatial signature of these mesoscale structures.

The impact of mesoscale circulation on nutrient distribution was likewise significant. The advection of warm, low-nutrient waters from northern circumpolar regions—likely mediated by these eddies—resulted in exceptionally low nitrate and phosphate concentrations north of the Polar Front, reaching levels nearly an order of magnitude below typical summer values (Fig. 2b; see section 4.2 for more details). South of the major fronts, the biogeochemical response was more nuanced: while nitrate and phosphate remained relatively high, silicate displayed steep meridional gradients, consistent with the established position of the silicate front. This spatial heterogeneity in nutrient availability appears to have governed the observed phytoplankton community composition and bloom dynamics.

In summary, our findings demonstrate that the onset and maintenance of the 2020 MHW in the Drake Passage were driven primarily by internal oceanic processes—specifically, the activity of energetic anticyclonic eddies—rather than by direct atmospheric heat input. These eddy features not only structured the thermal characteristics of the upper ocean but also modulated the spatial distribution of key nutrients, fundamentally shaping the biogeochemical and ecological environment experienced by primary producers. A deeper understanding of the coupling between mesoscale circulation, nutrient fluxes, and biological responses is essential for predicting the sensitivity of Southern Ocean ecosystems in an era of rapid, dynamic warming.

### 4.2 Nutrient distributions

The meridional nutrient distributions documented during the POWELL-2020 campaign reflected the changes in water masses depicted by the Southern Ocean fronts. The sharp silicate gradient identified at the Polar Front in both the northbound and southbound transits (Fig. 3b), also known as the Silicate Front, represents the transition between silicate-poor waters to the north and silicate-rich waters to the south (e.g. Trull et al., 2018; Freeman et al., 2019). The poleward increase in nitrate and phosphate concentrations across the Drake Passage in both transits is also consistent with that documented in previous reports (Freeman et al., 2019). However, it is important to note that concentrations for nitrate and phosphate during the POWELL-2020 expedition were lower than average summer values for all the circumpolar systems (Table 1). The anomalously low concentrations, were particularly evident for the case of nitrate during the northbound transit, when nitrate concentrations in most of the AZ and in the PFZ and SAZ were one order of magnitude lower than average summer concentrations (Table 1; Freeman et al., 2019).

The low temporal variability in silicate concentration in the PFZ and AAZ between the southbound and northbound transits contrasts with the substantial variations in diatom cell concentrations in the same zonal systems (i.e. between early January and late-January and early-February). As explained in further detail in section 4.4., a diatom bloom was documented in the SZ and AAZ during the northbound transit, and therefore, the lack of enhanced silicate consumption could be considered difficult to reconcile. However, looking in detail into the makeup of the diatom assemblage gives us some hints to reconcile these results. The main

604

605

606

607

608

609

610

611

612

613

614

615

616

617

618

619

620

621

622

623

624

625

626

627

628 629

630

631

632

633

634

635

636

637

638

639

640

641

642

643

644

645

646

647

648





components of the diatom bloom documented during the northbound transit were small *Fragilariopsis* species (e.g. the apical axis length of *F. pseudonana* is 4-11  $\mu$ m length in our study region; Cefarelli et al., 2010) that are characterized with a substantially lower silica requirement than larger, robustly silicified diatoms such as *F. kerguelensis* (apical length ranging from 17 to 83  $\mu$ m; Cefarelli et al., 2010). This feature, together with the rapid silicate recycling of the frustules of small *Fragilariopsis* species in the upper water column (Grigorov et al., 2014; Rigual-Hernández et al., 2016) seems to be sufficient to sustain high diatom cell concentrations without a remarkable silica consumption.

Under iron-replete conditions, diatoms use silicate and nitrate in a molar ratio of 1:1, which results in a balanced drawdown of both nutrients in diatom-dominated environments (Brzezinski, 1985). However, iron-deficient conditions, which limits phytoplankton growth across much of the Southern Ocean (Tagliabue et al., 2014), lead to an enhanced consumption of silicate over nitrate, with silicate to nitrate molar ratios of 2:1 or greater (Hutchins and Bruland, 1998; Takeda, 1998; Franck et al., 2000; Hutchins et al., 2001). Therefore, two possible processes alone or in combination could explain the pronounced decrease in nitrate but steady silicate concentrations observed in the Drake Passage between the southbound and northbound transits (Fig. 3). The first one is the advection of nitrate poor waters from lower latitudes into the Drake Passage. The outermost circumpolar systems of the Southern Ocean and waters of the southern Pacific Ocean are characterized by lower nitrate levels than those in the southern Drake Passage (Freeman et al., 2019). Alternatively, or complimentarily, a phytoplankton group other than diatoms might be responsible for a substantial fraction of the nitrate drawdown. As coccolithophore abundance was negligible in the AAZ (Fig. 6) and their abundance substantially decreased in the Drake Passage between the southbound and northbound transit, it is unlikely that coccolithophore proliferation was responsible for the nitrate drawdown during the warm water event. In turn, the soft-body and colonial Prymnesiophyte Phaeocystis antarctica and/or dinoflagellates are likely suspects as they do not require silicate for their growth and can account for a substantial fraction of algal biomass in the Southern Ocean (Kopczyńska and Ligowski, 1982; Liebezeit, 1987; Smith Jr. and Gordon, 1997; Arrigo et al., 1999; de Salas et al., 2011; Eriksen et al., 2018, among others). It should be noted that meltwater input from sea ice with low nitrate concentration could also lead to low nitrate concentration due to the due to the dilution of nitrate in surface waters (Servettaz et al., 2025). However, since the drop in nitrate levels occurs in the AAZ (station 121) which is a region characterized by little influence of sea ice in the during summer in the Drake Passage (Fig. 3), the possibility of sea ice melting dilution driving the low nitrate levels observed during the northbound transit in the POWELL-2020 is unlikely.

# 4.3 Phytoplankton abundance and species distribution

Overall, the abundance and distribution of the phytoplankton assemblages across the Drake Passage and Bransfield Strait mirrored the changes in the physical and chemical properties of the water column delineated by the fronts. The increase in diatom abundance south of the PF (Fig. 4) is directly related to the increase in silicate concentrations in the water column that fuel diatom productivity (Landry et al., 2002; Wright et al., 2010; Assmy et al., 2013; Trull et al., 2018). The dominance of *F. kerguelensis* in the Subantarctic Zone and Polar Frontal Zones (i.e., north of the PF) agrees well with previous work in the southwestern Atlantic Ocean where peak relative abundance of this species were documented in the Drake Passage (Cefarelli et al., 2010). However, the meridional distribution in our study is somewhat different from that documented in the southcentral Atlantic, where Froneman et al. (1995) observed maximum contributions of *F. kerguelensis* south of the Polar Front (i.e. an opposite trend to that observed here; Fig. 4). The





reason for this discrepancy is most likely due to the proliferation of small *Fragilariopsis* species in the southern Drake Passage. Interestingly, *F. kerguelensis* dominated in areas characterized by low silicate (< 4  $\mu$ mol L<sup>-1</sup>) and low iron levels (Supplementary Figure 3) during both the southbound and northbound transits. This finding is surprising because the growth rate of large and heavily silicified diatoms such as *F. kerguelensis* are limited at silicate concentrations below 5  $\mu$ M and substantially curtailed below 2.5  $\mu$ M (Frank et al., 2000).

The distribution of *F. cylindrus/nana* during the POWELL-2020 campaign is consistent with previous reports that documented the dominance of *F. cylindrus/nana* in the southern Drake Passage and Weddell Sea (Kang and Fryxell, 1992; Kang and Fryxell, 1993; Cefarelli et al., 2010). Moreover, our results underscore the strong affinity of this species towards regions under the influence of sea ice, as previously reported in both water column and seafloor sediments (Leventer, 1992; Zielinski and Gersonde, 1997; Armand et al., 2005, among others). Likewise, the important contribution of *F. pseudonana* in the AAZ and SZ, in both early January and late January-early February, is in agreement with previous research that reported this species as a major component of the diatom communities during summer in the Drake Passage (Kang and Lee, 1995; Cefarelli et al., 2010) and NW Elephant Island (the most northerly of the South Shetland Islands, Villafañe et al., 1995). This species has been also described as an important contributor of the diatom assemblages in the high-nutrient, low-chlorophyll (HNLC) waters off Kerguelen Archipelago (Armand et al., 2008) and as part of the sinking diatom assemblages collected by sediment traps in AZ south of Tasmania (Rigual-Hernández et al., 2015), suggesting the capacity of this species to also thrive under low iron levels.

The low contribution of *Chaetoceros* RS in our survey contrasts with the high abundance of this taxon in the surface sediments of the Bransfield Strait (> 400 10<sup>6</sup> valves g¹ of dry sediment; Crosta et al., 1997). *Chaetoceros* RS formation has been related to nitrogen depletion and/or light limitation (Bodungen et al., 1986; Kuwata and Takahashi, 1990; Leventer, 1991a). In particular, silicon to nitrate molar ratios above 9.3 have been documented to trigger resting spore formation in *Chaetoceros* populations (Kuwata and Takahashi, 1990). The only neritic stations (i.e. the habitat of the resting spore forming *Chaetoceros* subgenus *Hyalochaeta*) with relatively high silicon to nitrogen ratios during our survey were those in the Bransfield Strait with values ranging from 4.4 to 8.4. Despite these relatively high values, only in the stations South Bay of Livingston Island some *Chaetoceros* RS were registered in concentrations above 5%. Taken together, all the above indicate that the interplay of more environmental factors aside from nitrogen limitation (e.g. light limitation) are required to trigger *Chaetoceros* RS formation in the Bransfield Strait. It is likely that the moment of the sampling was too early or too late in the seasonal succession to capture the formation of resting spores by *Chaetoceros* populations in the neritic habitats of the Antarctic Peninsula (Leventer, 1991b).

The co-occurrence of the epiphytic and sea-ice affiliated *P. kamtschaticum* (Medlin, 1990; Scott and Marchant, 2005; Majewska et al., 2015) with elevated concentrations of fine sediments in the coastal waters of Livingston Island, is a clear reflection of the affinity of this species for glacial meltwater discharge. These results highlight the potential of this species as proxy for glacial meltwater discharge in the paleorecord. Moreover, the co-occurrence of peak relative contribution of *Navicula* spp. in the same stations also suggests that this taxon was also associated to the sediment input from subglacial waters (Fig. 4e). However, the utility of this genus as a proxy for glacial discharge should be made with caution as this genus contains species both benthic and planktonic (Al-Handal and Wulff, 2008; Majewska et al., 2015; Rigual-Hernández et al., 2015; Daglio et al., 2018; Silva et al., 2019).





Lastly, although the resolution of our light microscopy analysis was not sufficient to resolve the identification of small centric diatoms (grouped here as small centric <  $20 \, \mu m$  group; Fig. 4f), SEM analysis of selected samples indicate that, at least some of the specimens were *Minidiscus chilensis*. This species had been previously documented in large numbers in the western Bransfield Strait (Kang et al., 2003) and Ryder Bay (Annett et al., 2010). Owing to the relevant contribution of the small centric group in some samples during the POWELL-2020 expedition (Fig. 4f) and the potential relevant role of *Minidiscus* in the biological pump of the region (Leblanc et al., 2018), we recommend including the identification of small diatom species in future surveys in the AP.

In terms of coccolithophore distributions, the observed latitudinal pattern (i.e. coccolithophores were most abundant north of the PF) is consistent with previous reports in the Drake Passage and AP (Charalampopoulou et al., 2016; Saavedra-Pellitero et al., 2019) and in other sectors of the Southern Ocean (Cubillos et al., 2007; Malinverno et al., 2015; Saavedra-Pellitero and Baumann, 2015; Patil et al., 2017; Rigual Hernández et al., 2018; Trull et al., 2018; Rigual-Hernández et al., 2020b, among others). The substantially lower cell numbers than those of diatoms, together with the small size of their coccospheres indicate that coccolithophores must account for only a small fraction of the algal biomass during our survey. This observation is consistent with previous studies where coccolithophore contribution to total phytoplankton biomass accumulation has been shown to be small, accounting for less than 10% in subantarctic waters and less than 1% in Antarctic waters (Trull et al., 2018). Among all the environmental parameters controlling coccolithophore distribution, temperature has been suggested to play a major role their latitudinal distribution in the Southern Ocean (Boyd et al., 2010; Feng et al., 2017; Rigual-Hernández et al., 2020a). Moreover, temperature also represents a major control for coccolithophore diversity (Rigual-Hernández et al., 2020b), with assemblages turning nearly or entirely monospecific south of the PF (Cubillos et al., 2007; Malinverno et al., 2015; Patil et al., 2017; Rigual Hernández et al., 2018; Saavedra-Pellitero et al., 2019).

### 4.4 Influence of the warm water anomaly on the phytoplankton communities

Our data suggests that the anomalously high SSTs (up to +3°C; Fig. 3a) recorded during the northbound transit were driven by the advection of an anticyclonic eddy from the northernmost systems of the Drake Passage. Eddy and meander formation in the Subantarctic Zone and their subsequent transport across the Polar Front is a frequent phenomenon in the Southern Ocean in general (Hogg et al., 2008), and in the Drake Passage (Meredith and Hogg, 2006) and the Weddell-Scotia confluence (Kahru et al., 2007), in particular. This idea is supported by the presence of *Chaetoceros* resting spores as south as the AAZ during the northbound transit. Since the habitat of *Chaetoceros* subgenus *Hyalochaete* is restricted to coastal and inshore waters (Hasle and Syvertsen, 1997), the presence of the vegetative and/or resting spores of this taxon can be taken as an indicator of influence of coastal environments (e.g. Lange et al., 1994; Treppke et al., 1996; Wilks et al., 2021). Therefore, the presence of *Chaetoceros* resting spores coupled with the warm water anomaly in the AAZ (Fig. 4d) is interpreted as the lateral advection of water masses off South America continental shelf.

Notably, as mentioned in section 4.2, the temperature anomaly was also coupled with a pronounced drawdown in nitrate concentrations from the AAZ and northwards (Fig. 3b). We interpret the anomalously low nitrate concentrations as a result of limited vertical nutrient supply to the euphotic zone induced by warming together with a steady consumption of

741

742

743

744 745

746

747

748

749

750

751

752

753

754

755

756

757

758 759

760

761

762

763

764

765 766

767

768

769

770

771

772

773

774

775

776

777

778

779

780

781

782

783

784

785





nutrients by phytoplankton. This hypothesis is highly likely as anomalous warming events such as MHWs generally drive a reduction of mixed layer depths (Amaya et al., 2021; Oliver et al., 2021) and widespread surface nutrient declines in subpolar and polar ecosystems (e.g. Peña et al., 2019; Servettaz et al., 2025). However, aside from a reduction of nutrient supply, enhanced nutrient consumption by phytoplankton would be required to explain the unusually low nitrate concentrations observed during the northbound transit (Fig. 3 and Table 1). The enhanced diatom concentrations observed in the SZ and AAZ in late-January early-February (up to ca. 5 x 10<sup>6</sup> cells L<sup>-1</sup>) were one to three orders of magnitude greater than previous reports in the same zonal systems in the AP during summer (Villafañe et al., 1995; Olguin et al., 2006; Cefarelli et al., 2010). These results suggests that the bloom of small size diatom species may have been responsible or largely contributed for the nutrient depletion south of the Polar Front. This notion is in agreement with some studies in the Antarctic Peninsula where anomalously low nitrate concentrations (below 5 µM L<sup>-1</sup>) had been reported associated with the development of intense phytoplankton blooms (Holm-Hansen et al., 1989; Karl et al., 1991; Servettaz et al., 2025). It is important to note that the diatom bloom in the SZ and AAZ was not coupled with a remarkable increase in chlorophyll-a concentration. This mismatch can be attributed to two main factors. Firstly, other phytoplankton functional groups (e.g. Cryptophytes and Prymnesiophytes) can contribute substantially to the total chlorophyll-a production in the study region (Moline et al., 2004; Montes-Hugo et al., 2008). Therefore, changes in the relative contribution of these groups throughout our survey could have contributed to the lack of strong relationship between diatom numbers and chlorophyll-a concentration. Secondly, diatom assemblages display a wide range of sizes with cellular biovolumes spanning up to over nine orders of magnitude in the world ocean (Leblanc et al., 2012). Therefore, a shift in the proportions of the dominant diatom species does not necessarily imply a proportional change in the chlorophyll-a signal, as the amount of chlorophyll-a content across species may vary substantially (Chan, 1978).

The increase of one order of magnitude of the average diatom cell concentration in the SZ and AAZ between the southbound and northbound transits (from 2 x 105 to 1.8 x 106, respectively; Fig. 4a) is consistent with the results of incubation experiments with one of the main components of the bloom: F. cylindrus/nana. In particular, warming has a positive effect on the growth rates of F. cylindrus (Antoni et al., 2020) while decreasing its iron requirements (Jabre and Bertrand, 2020). These characteristics seems to have provided an ecological advantage over the rest of the diatom assemblage as also reflected by the increase in the relative contribution of this species during the northbound transit. Likewise, the observed increase in the absolute abundance of F. pseudonana also suggests that the warmer water conditions during the heat wave also stimulated the growth of this species although to a lower extent than for F. cylindrus/nana. However, it could be argued that the observed increase in diatom abundance in the southern Drake Passage between early January and late January could be the result of the regular seasonal progression of diatom productivity. Chlorophyll-a climatology (years 1998-2022) for the southern Drake Passage estimated by Ferreira et al. (2024) reveals that average algal biomass accumulation between early January and early February during is almost identical (less than 0.1 mg Chl-a m<sup>-3</sup> difference between them). Assuming a similar relative contribution of diatoms to the total Chl-a signal between January and February, a similar diatom abundance concentration could be expected in early January and in early February during a regular year. It follows that the enhanced abundance in diatom concentrations documented during the northbound transit was most likely the result of an exceptional event rather than the regular phenological response of diatoms in this region.

787

788

789

790

791 792

793

794

795

796

797

798

799

800

801

802

803

804

805

806

807

808

809

810

811

812

813

814

815

816

817

818

819

820

821

822

823

824

825

826

827

828

829

830

831

832





In regard to the possible influence of the anomalous warming event on coccolithophores populations, it is worth noting that average coccolithophore abundance decreased two-fold in the SAZ and PFZ during this event compared with the observations made in the southbound transit (Fig. 5). Notably, coccolithophore concentrations were also substantially lower than previous reports during the austral summer in both the SAZ (23 x 10<sup>4</sup> coccospheres L<sup>-1</sup>, Charalampopoulou et al. 2016; 15 x 10<sup>4</sup> coccospheres L<sup>-1</sup>, Saavedra-Pellitero et al. 2019) and PFZ (58 x 10<sup>4</sup> coccospheres L<sup>-1</sup>, Charalampopoulou et al. 2016; 11 x 10<sup>4</sup> coccospheres L<sup>-1</sup>, Saavedra-Pellitero et al. 2019). Therefore, it could be speculated that the warm water anomaly may be responsible for the low coccolithophore productivity. As mentioned before, both laboratory experiments (Feng et al., 2017) and field evidence (Rivero-Calle et al., 2015) have underscored the primary role of temperature in the control of coccolithophore growth rates. However, according to these studies, an increase of SSTs would imply an increase of growth rates, which is opposite to what we observed during the POWELL-2020 campaign. It follows that different environmental controls other than temperature must have been responsible for the decrease in coccolithophore abundance within the SAZ and PFZ. Notably, Trull et al. (2018) indicated that macronutrient availability could be an important factor determining the growth of coccolithophores in oligotrophic waters at the northern edge of the Southern Ocean. This idea is reinforced by laboratory culture experiments that revealed that nitrate concentration is a critical factor controlling the photosynthetic and growth rates of subantarctic E. huxleyi (Feng et al., 2017). The latter study also demonstrated that, in contrast to nitrate, the growth rate of E. huxleyi remained relatively constant across a wide range of phosphate concentrations. Taking into consideration all the above, it is likely that the drop of ca. one order of magnitude of nitrate concentrations (nitrate  $> 1.3 \mu M$ ) during the northbound transit could have been responsible for low coccolithophore abundance. Lastly, our data also suggests the change in nutrient concentrations and/or warming induced by the warm water anomaly favoured the development of C. leptoporus over E. huxleyi that is a good competitor for phosphate, but does not grow well under low nitrate levels (Egge and Heimdal, 1994).

Taken together all the above, our results suggest that an increase in the frequency of warm water anomalies could potentially favour the development of small diatom species in the southern circumpolar systems of the Southern Ocean and a decrease in coccolithophore numbers north of the PF. However, owing to low contribution of coccolithophore communities to phytoplankton biomass and their mild response to the warming event, it is likely that a moderate decrease in coccolithophore numbers does not represent a major impact for trophic chain or the biogeochemical cycles in the low productivity ecosystems where they thrive (i.e. mainly SAZ and PFZ). In turn, the more pronounced shifts in the abundance and composition of diatom communities, which often dominate algal biomass accumulation in the most productive ecosystems of Antarctica, are likely to be far reaching. An increase in the abundance of small diatom species is in agreement with in situ and model observations that indicate that warm water anomalies will result in an increasing importance of small size phytoplankton in the world's oceans (Acevedo-Trejos et al., 2014; Peña et al., 2019; Wyatt et al., 2022). This shift in the composition and average size reduction of phytoplankton communities is likely to have impacts in the food chain and efficiency of the biological pump. Previous studies indicate that an average reduction in the cell size of phytoplankton communities in the Antarctic Ocean could have important impact on the abundance of keystone zooplankton grazers, particularly salps and krill (Moline et al., 2008). Since krill feed mainly of phytoplankton cells larger than 10 µm, the overall size reduction of phytoplankton communities has resulted in a decrease of krill numbers and an increase in salp abundance (grazers unaffected by the size of their prey) (Moline et al., 2008).





Because krill represents the primarily food source for many Antarctic birds and mammals (Atkinson et al., 2004), a shift in the phytoplankton communities, and therefore krill abundance, is predicted to have a substantial negative effect on the krill-dependent food chain (Murphy et al., 2007, 2016). The effect in the of the biological pump is less clear. While small diatom are traditionally regarded as less efficient carbon vectors to the deep ocean owing to the fast remineralization in the upper water column (e.g. Legendre and Le Fèvre, 1995), some studies have challenged this view. Leblanc et al. (2018) demonstrated that small-sized diatom (2–20  $\mu$ m) can develop large blooms across the global ocean (including the Antarctic Peninsula) and reach the seafloor at high sinking rates, thereby contributing substantially to carbon sequestration. Therefore, the impact of an increase in the abundance of small size diatoms species in carbon sequestration in the Southern Ocean is still uncertain and remain to be quantified and parameterized.

### Conclusions

Our evidence, albeit circumstantial, suggests that extreme warming events in southernmost circumpolar systems of the Drake Passage can be driven by the advection of mesoscale anticyclonic eddies from lower latitudes. Notably, the unusually warmer conditions generated by these eddies can drive substantial changes in the abundance and structure of phytoplankton communities. Our results provide field-based evidence for observations made on culture experiments that indicate that the growth of small *Fragilariopsis* species is stimulated by warmer water temperatures. The remarkable nitrate drawdown observed in large swath of the Drake during the onset of the MHW indirectly suggests that warm water anomalies may favour the development of soft-tissue phytoplankton in the Drake Passage. Moreover, it is likely that the low nitrate levels resulted in a reduction of coccolithophore productivity north of the PF. As both the intensity and frequency of warm water anomalies are expected to increase in the Southern Ocean in the coming decades, an increase in the abundance smaller diatom taxa could be expected. This shift in the phytoplankton community structure, will most likely have an impact on higher trophic levels, particularly krill and salps, ultimately affecting higher trophic levels as well as the functioning of the marine carbon cycle.

### 861 Data availability

All data presented in the figures will be made available upon publication.

# Author contributions.

CE, FJJ and FB planned and led the POWELL-2020 campaign. AL, JAF, DE and JE performed the water sampling. MFB and GN obtained and interpreted satellite and modelled data. ASRH, AL and JAF led the phytoplankton study. ASRH, AL, MD and MAB performed the sample processing, microscopy and image analyses for characterization and quantification of the diatom assemblage. ASRH and JAF performed microscopy analysis for the characterization and quantification of the coccolithophore assemblage. JE and MS performed nutrient analyses. Manuscript writing was led by ASRH with substantial contributions and edits by MFB, GN and AL. All authors contributed to the interpretation of the data, manuscript review and editing.

### Acknowledgements

ARH and MB acknowledge funding from project BASELINE (PID2021-126495NB-741 C33) funded by the Spanish MCIN/AEI/10.13039/5011000110 33. CE and FB acknowledge funding from the





- AntOCEAN project PID2021- 126495NB-741 C31/C32 cofounded by the European Union through
- 877 FEDER funds. DE was funded by the UK Research and Innovation Engineering and Physical
- 878 Sciences Research Council (grant number EP/X02623X/1). Authors would like to thank the BIO-
- 879 Hespérides captain and crew and the UTM personnel for their hard work and technical assistance
- 880 during the cruise. Authors wish to thank Ms Jane Carskaddan and Mr Zach O'Donnell (Colgate
- 881 University) for assistance with scanning electron microscopy analyses and also Julia Gutiérrez-
- 882 Pastor for her assistance with water sampling. The authors thank all members of the Copernicus
- 883 Marine Service, the Copernicus Climate Change Service, and the ECMWF for providing satellite-
- 884 derived and modelled data essential to this work. We thank GEBCO for the GEBCO Grid 2024
- used as background for map in figure 1.

#### References

886

- 887 Acevedo-Trejos, E., Brandt, G., Steinacher, M., and Merico, A.: A glimpse into the future
- 888 composition of marine phytoplankton communities, Frontiers in Marine Science, 1,
- 889 10.3389/fmars.2014.00015, 2014.
- 890 Al-Handal, A. Y., and Wulff, A.: Marine epiphytic diatoms from the shallow sublittoral zone
- in Potter Cove, King George Island, Antarctica, 2008.
- 892 Amaya, D. J., Alexander, M. A., Capotondi, A., Deser, C., Karnauskas, K. B., Miller, A. J., and
- 893 Mantua, N. J.: Are long-term changes in mixed layer depth influencing North Pacific marine
- heatwaves?, Bulletin of the American Meteorological Society, 102, S59-S66, 2021.
- 895 Aminot, A., Kérouel, R., and Coverly, S. C.: Nutrients in seawater using segmented flow
- analysis, in: Practical guidelines for the analysis of seawater, CRC press, 143-178, 2009.
- 897 Annett, A. L., Carson, D. S., Crosta, X., Clarke, A., and Ganeshram, R. S.: Seasonal
- 898 progression of diatom assemblages in surface waters of Ryder Bay, Antarctica, Polar Biol,
- 899 33, 13-29, 10.1007/s00300-009-0681-7, 2010.
- 900 Annett, A. L., Fitzsimmons, J. N., Séguret, M. J. M., Lagerström, M., Meredith, M. P.,
- 901 Schofield, O., and Sherrell, R. M.: Controls on dissolved and particulate iron distributions
- 902 in surface waters of the Western Antarctic Peninsula shelf, Marine Chemistry, 196, 81-97,
- 903 <a href="https://doi.org/10.1016/j.marchem.2017.06.004">https://doi.org/10.1016/j.marchem.2017.06.004</a>, 2017.
- 904 Antoni, J. S., Almandoz, G. O., Ferrario, M. E., Hernando, M. P., Varela, D. E., Rozema, P. D.,
- 905 Buma, A. G., Paparazzo, F. E., and Schloss, I. R.: Response of a natural Antarctic
- 906 phytoplankton assemblage to changes in temperature and salinity, Journal of
- 907 Experimental Marine Biology and Ecology, 532, 151444, 2020.
- 908 Ardelan, M. V., Holm-Hansen, O., Hewes, C. D., Reiss, C. S., Silva, N. S., Dulaiova, H.,
- 909 Steinnes, E., and Sakshaug, E.: Natural iron enrichment around the Antarctic Peninsula in
- 910 the Southern Ocean, Biogeosciences, 7, 11-25, 10.5194/bg-7-11-2010, 2010.
- 911 Armand, L. K., Crosta, X., Romero, O., and Pichon, J.-J.: The biogeography of major diatom
- 912 taxa in Southern Ocean sediments: 1. Sea ice related species, Palaeogeography,
- 913 Palaeoclimatology, Palaeoecology, 223, 93-126,
- 914 http://dx.doi.org/10.1016/j.palaeo.2005.02.015, 2005.
- 915 Armand, L. K., Cornet-Barthaux, V., Mosseri, J., and Quéguiner, B.: Late summer diatom
- 916 biomass and community structure on and around the naturally iron-fertilised Kerguelen
- 917 Plateau in the Southern Ocean, Deep Sea Research Part II: Topical Studies in
- 918 Oceanography, 55, 653-676, http://dx.doi.org/10.1016/j.dsr2.2007.12.031, 2008.
- 919 Arrigo, K. R., Robinson, D. H., Worthen, D. L., Dunbar, R. B., DiTullio, G. R., VanWoert, M.,
- 920 and Lizotte, M. P.: Phytoplankton Community Structure and the Drawdown of Nutrients
- 921 and CO2 in the Southern Ocean, Science, 283, 365-367, 10.1126/science.283.5400.365,
- 922 1999.
- 923 Assmy, P., Smetacek, V., Montresor, M., Klaas, C., Henjes, J., Strass, V. H., Arrieta, J. M.,
- 924 Bathmann, U., Berg, G. M., Breitbarth, E., Cisewski, B., Friedrichs, L., Fuchs, N., Herndl, G.
- 925 J., Jansen, S., Krägefsky, S., Latasa, M., Peeken, I., Röttgers, R., Scharek, R., Schüller, S. E.,





- 926 Steigenberger, S., Webb, A., and Wolf-Gladrow, D.: Thick-shelled, grazer-protected
- 927 diatoms decouple ocean carbon and silicon cycles in the iron-limited Antarctic
- 928 Circumpolar Current, Proceedings of the National Academy of Sciences, 110, 20633-
- 929 20638, 10.1073/pnas.1309345110, 2013.
- 930 Atkinson, A., Siegel, V., Pakhomov, E., and Rothery, P.: Long-term decline in krill stock and
- increase in salps within the Southern Ocean, Nature, 432, 100-103, 2004.
- 932 Ballerini, T., Hofmann, E. E., Ainley, D. G., Daly, K., Marrari, M., Ribic, C. A., Smith Jr, W. O.,
- 933 and Steele, J. H.: Productivity and linkages of the food web of the southern region of the
- 934 western Antarctic Peninsula continental shelf, Progress in Oceanography, 122, 10-29,
- 935 2014
- 936 Beech, N., Rackow, T., Semmler, T., Danilov, S., Wang, Q., and Jung, T.: Long-term
- 937 evolution of ocean eddy activity in a warming world, Nature Climate Change, 12, 910-917,
- 938 10.1038/s41558-022-01478-3, 2022.
- 939 Bell, J. J., Micaroni, V., Strano, F., Ryan, K. G., Mitchell, K., Mitchell, P., Wilkinson, S.,
- 940 Thomas, T., Bachtiar, R., and Smith, R. O.: Marine heatwave-driven mass mortality and
- 941 microbial community reorganisation in an ecologically important temperate sponge,
- 942 Global change biology, 30, e17417, 2024.
- 943 Bendschneider, K., and Robinson, R. J.: A new spectrophotometric method for the
- 944 determination of nitrite in sea water, 1952.
- 945 Bertolin, M. L., and Schloss, I. R.: Phytoplankton production after the collapse of the
- 946 Larsen A Ice Shelf, Antarctica, Polar Biol, 32, 1435-1446, 2009.
- 947 Bian, C., Jing, Z., Wang, H., Wu, L., Chen, Z., Gan, B., and Yang, H.: Oceanic mesoscale
- 948 eddies as crucial drivers of global marine heatwaves, Nature Communications, 14, 2970,
- 949 10.1038/s41467-023-38811-z, 2023.
- 950 Blanchard-Wrigglesworth, E., Roach, L. A., Donohoe, A., and Ding, Q.: Impact of Winds
- 951 and Southern Ocean SSTs on Antarctic Sea Ice Trends and Variability, Journal of Climate,
- 952 34, 949-965, <a href="https://doi.org/10.1175/JCLI-D-20-0386.1">https://doi.org/10.1175/JCLI-D-20-0386.1</a>, 2021.
- 953 Bodungen, B. v., Smetacek, V. S., Tilzer, M. M., and Zeitzschel, B.: Primary production and
- 954 sedimentation during spring in the Antarctic Peninsula region, Deep Sea Research Part A.
- 955 Oceanographic Research Papers, 33, 177-194, 1986.
- 956 Bond, N. A., Cronin, M. F., Freeland, H., and Mantua, N.: Causes and impacts of the 2014
- 957 warm anomaly in the NE Pacific, Geophysical Research Letters, 42, 3414-3420,
- 958 <a href="https://doi.org/10.1002/2015GL063306">https://doi.org/10.1002/2015GL063306</a>, 2015.
- 959 Boyd, P., and Trull, T.: Understanding the export of biogenic particles in oceanic waters: Is
- there consensus?, Progress in Oceanography, 72, 276-312, 2007.
- 961 Boyd, P. W., Strzepek, R., Fu, F., and Hutchins, D. A.: Environmental control of open-ocean
- 962 phytoplankton groups: Now and in the future, Limnology and Oceanography, 55, 1353-
- 963 1376, 10.4319/lo.2010.55.3.1353, 2010.
- 964 Brzezinski, M. A.: The Si:C:N ratio of marine diatoms: Interspecific variability and the effect
- of some environmental variables, Journal of Phycology, 21, 347-357, 10.1111/j.0022-
- 966 3646.1985.00347.x, 1985.
- 967 Cavole, L. M., Demko, A. M., Diner, R. E., Giddings, A., Koester, I., Pagniello, C. M., Paulsen,
- 968 M.-L., Ramirez-Valdez, A., Schwenck, S. M., and Yen, N. K.: Biological impacts of the 2013-
- 969 2015 warm-water anomaly in the Northeast Pacific: winners, losers, and the future,
- 970 Oceanography, 29, 273-285, 2016.
- 971 Cefarelli, A. O., Ferrario, M. E., Almandoz, G. O., Atencio, A. G., Akselman, R., and Vernet,
- 972 M.: Diversity of the diatom genus Fragilariopsis in the Argentine Sea and Antarctic waters:
- 973 morphology, distribution and abundance, Polar Biol, 33, 1463-1484, 10.1007/s00300-010-
- 974 0794-z, 2010.
- 975 Chan, A. T.: COMPARATIVE PHYSIOLOGICAL STUDY OF MARINE DIATOMS AND
- 976 DINOFLAGELLATES IN RELATION TO IRRADIANCE AND CELL SIZE. I. GROWTH UNDER





- 977 CONTINUOUS LIGHT, Journal of Phycology, 14, 396-402, https://doi.org/10.1111/j.1529-
- 978 <u>8817.1978.tb02458.x</u>, 1978.
- 979 Charalampopoulou, A., Poulton, A. J., Bakker, D. C., Lucas, M. I., Stinchcombe, M. C., and
- 980 Tyrrell, T. J. B.: Environmental drivers of coccolithophore abundance and calcification
- 981 across Drake Passage (Southern Ocean), 13, 5917-5935, 2016.
- 982 Cook, A., Fox, A., Vaughan, D., and Ferrigno, J.: Retreating glacier fronts on the Antarctic
- 983 Peninsula over the past half-century, Science, 308, 541-544, 2005.
- 984 Crosta, X., Pichon, J.-J., and Labracherie, M.: Distribution of Chaetoceros resting spores in
- 985 modern peri-Antarctic sediments, Marine Micropaleontology, 29, 283-299, 1997.
- 986 Cubillos, J., Wright, S., Nash, G., De Salas, M., Griffiths, B., Tilbrook, B., Poisson, A., and
- 987 Hallegraeff, G.: Calcification morphotypes of the coccolithophorid Emiliania huxleyi in the
- 988 Southern Ocean: changes in 2001 to 2006 compared to historical data, Marine Ecology
- 989 Progress Series, 348, 47-54, 2007.
- 990 Daglio, Y., Sacristán, H., Ansaldo, M., and Rodríguez, M. C.: Benthic diatoms from Potter
- 991 Cove, 25 de Mayo (King George) Island, Antarctica: Mucilage and glucan storage as a C-
- 992 source for limpets, Polar Science, 15, 39-48, https://doi.org/10.1016/j.polar.2018.01.004,
- 993 2018.
- 994 Davison, B. J., Hogg, A. E., Moffat, C., Meredith, M. P., and Wallis, B. J.: Widespread
- 995 increase in discharge from west Antarctic Peninsula glaciers since 2018, The Cryosphere,
- 996 18, 3237-3251, 2024.
- 997 de Salas, M. F., Eriksen, R., Davidson, A. T., and Wright, S. W.: Protistan communities in the
- 998 Australian sector of the Sub-Antarctic Zone during SAZ-Sense, Deep Sea Research Part II:
- 999 Topical Studies in Oceanography, 58, 2135-2149,
- 1000 <a href="http://dx.doi.org/10.1016/j.dsr2.2011.05.032">http://dx.doi.org/10.1016/j.dsr2.2011.05.032</a>, 2011.
- 1001 Deppeler, S. L., and Davidson, A. T.: Southern Ocean Phytoplankton in a Changing
- 1002 Climate, Frontiers in Marine Science, 4, 10.3389/fmars.2017.00040, 2017.
- 1003 Eakin, C. M., Sweatman, H. P., and Brainard, R. E.: The 2014–2017 global-scale coral
- bleaching event: insights and impacts, Coral Reefs, 38, 539-545, 2019.
- 1005 Eayrs, C., Holland, D., Francis, D., Wagner, T., Kumar, R., and Li, X.: Understanding the
- 1006 Seasonal Cycle of Antarctic Sea Ice Extent in the Context of Longer-Term Variability,
- 1007 Reviews of Geophysics, 57, 1037-1064, https://doi.org/10.1029/2018RG000631, 2019.
- 1008 Egge, J. K., and Heimdal, B. R.: Blooms of phytoplankton including Emiliania huxleyi
- 1009 (Haptophyta). Effects of nutrient supply in different N: P ratios, Sarsia, 79, 333-348,
- 1010 10.1080/00364827.1994.10413565, 1994.
- 1011 Eppley, R.: Temperature and phytoplankton growth in the sea, Fishery Bulletin, 70, 1063-
- 1012 1085, 1972.
- 1013 Eriksen, R., Trull, T. W., Davies, D., Jansen, P., Davidson, A. T., Westwood, K., and van den
- 1014 Enden, R.: Seasonal succession of phytoplankton community structure from autonomous
- 1015 sampling at the Australian Southern Ocean Time Series (SOTS) observatory, Marine
- 1016 Ecology Progress Series, 589, 13-31, 2018.
- 1017 Feng, Y., Roleda, M. Y., Armstrong, E., Boyd, P. W., and Hurd, C. L.: Environmental controls
- 1018 on the growth, photosynthetic and calcification rates of a Southern Hemisphere strain of
- 1019 the coccolithophore Emiliania huxleyi, Limnology and Oceanography, 62, 519-540,
- 1020 10.1002/lno.10442, 2017.
- 1021 Fernández-Barba, M., Belyaev, O., Huertas, I. E., and Navarro, G.: Marine heatwaves in a
- 1022 shifting Southern Ocean induce dynamical changes in primary production,
- 1023 Communications Earth & Environment, 5, 404, 2024.
- 1024 Ferreira, A., Mendes, C. R., Costa, R. R., Brotas, V., Tavano, V. M., Guerreiro, C. V., Secchi,
- 1025 E. R., and Brito, A. C.: Climate change is associated with higher phytoplankton biomass
- 1026 and longer blooms in the West Antarctic Peninsula, Nature Communications, 15, 6536,
- 1027 2024.





- 1028 Franck, V., Brzezinski, M. A., Coale, K. H., and Nelson, D. M.: Iron and silicic acid
- 1029 concentrations regulate Si uptake north and south of the Polar Frontal Zone in the Pacific
- 1030 Sector of the Southern Ocean, Deep Sea Research Part II: Topical Studies in
- 1031 Oceanography, 47, 3315-3338, http://dx.doi.org/10.1016/S0967-0645(00)00070-9, 2000.
- 1032 Freeman, N. M., Munro, D. R., Sprintall, J., Mazloff, M. R., Purkey, S., Rosso, I., DeRanek, C.
- 1033 A., and Sweeney, C.: The observed seasonal cycle of macronutrients in Drake Passage:
- 1034 Relationship to fronts and utility as a model metric, Journal of Geophysical Research:
- 1035 Oceans, 124, 4763-4783, 2019.
- 1036 Frölicher, T. L., Fischer, E. M., and Gruber, N.: Marine heatwaves under global warming,
- 1037 Nature, 560, 360-364, 10.1038/s41586-018-0383-9, 2018.
- 1038 Froneman, P. W., Perissinotto, R., McQuaid, C. D., and Laubscher, R. K.: Summer
- 1039 distribution of netphytoplankton in the Atlantic sector of the Southern Ocean, Polar Biol,
- 1040 15, 77-84, 10.1007/BF00241045, 1995.
- 1041 Gao, G., Zhao, X., Jiang, M., and Gao, L.: Impacts of marine heatwaves on algal structure
- 1042 and carbon sequestration in conjunction with ocean warming and acidification, Frontiers
- 1043 in Marine Science, 8, 758651, 2021.
- 1044 Garrabou, J., Gómez-Gras, D., Medrano, A., Cerrano, C., Ponti, M., Schlegel, R.,
- 1045 Bensoussan, N., Turicchia, E., Sini, M., Gerovasileiou, V., Teixido, N., Mirasole, A.,
- 1046 Tamburello, L., Cebrian, E., Rilov, G., Ledoux, J.-B., Souissi, J. B., Khamassi, F., Ghanem,
- 1047 R., Benabdi, M., Grimes, S., Ocaña, O., Bazairi, H., Hereu, B., Linares, C., Kersting, D. K., la
- 1048 Rovira, G., Ortega, J., Casals, D., Pagès-Escolà, M., Margarit, N., Capdevila, P., Verdura, J.,
- 1049 Ramos, A., Izquierdo, A., Barbera, C., Rubio-Portillo, E., Anton, I., López-Sendino, P., Díaz,
- 1050 D., Vázquez-Luis, M., Duarte, C., Marbà, N., Aspillaga, E., Espinosa, F., Grech, D., Guala, I.,
- 1051 Azzurro, E., Farina, S., Cristina Gambi, M., Chimienti, G., Montefalcone, M., Azzola, A.,
- 1052 Mantas, T. P., Fraschetti, S., Ceccherelli, G., Kipson, S., Bakran-Petricioli, T., Petricioli, D.,
- 1053 Jimenez, C., Katsanevakis, S., Kizilkaya, I. T., Kizilkaya, Z., Sartoretto, S., Elodie, R., Ruitton,
- 1054 S., Comeau, S., Gattuso, J.-P., and Harmelin, J.-G.: Marine heatwaves drive recurrent mass
- 1055 mortalities in the Mediterranean Sea, Global Change Biology, 28, 5708-5725,
- 1056 https://doi.org/10.1111/gcb.16301, 2022.
- 1057 Gorodetskaya, I. V., Durán-Alarcón, C., González-Herrero, S., Clem, K. R., Zou, X., Rowe,
- 1058 P., Rodriguez Imazio, P., Campos, D., Leroy-Dos Santos, C., Dutrievoz, N., Wille, J. D.,
- 1059 Chyhareva, A., Favier, V., Blanchet, J., Pohl, B., Cordero, R. R., Park, S.-J., Colwell, S.,
- 1060 Lazzara, M. A., Carrasco, J., Gulisano, A. M., Krakovska, S., Ralph, F. M., Dethinne, T., and
- 1061 Picard, G.: Record-high Antarctic Peninsula temperatures and surface melt in February
- 1062 2022: a compound event with an intense atmospheric river, npj Climate and Atmospheric
- 1063 Science, 6, 202, 10.1038/s41612-023-00529-6, 2023.
- 1064 Gossart, A., Helsen, S., Lenaerts, J., Broucke, S. V., Van Lipzig, N., and Souverijns, N.: An
- 1065 evaluation of surface climatology in state-of-the-art reanalyses over the Antarctic Ice
- 1066 Sheet, Journal of Climate, 32, 6899-6915, 2019.
- 1067 Green, J., Heimdal, B., Paasche, E., and Moate, R.: Changes in calcification and the
- 1068 dimensions of coccoliths of Emiliania huxleyi (Haptophyta) grown at reduced salinities,
- 1069 Phycologia, 37, 121-131, 1998.
- 1070 Grigorov, I., Rigual-Hernandez, A. S., Honjo, S., Kemp, A. E. S., and Armand, L. K.: Settling
- 1071 fluxes of diatoms to the interior of the antarctic circumpolar current along 170°W, Deep
- 1072 Sea Research Part I: Oceanographic Research Papers, 93, 1-13,
- 1073 <a href="http://dx.doi.org/10.1016/j.dsr.2014.07.008">http://dx.doi.org/10.1016/j.dsr.2014.07.008</a>, 2014.
- 1074 Gutierrez-Villanueva, M. O., Chereskin, T. K., and Sprintall, J.: Upper-ocean eddy heat flux
- 1075 across the Antarctic Circumpolar Current in Drake Passage from observations: Time-mean
- 1076 and seasonal variability, Journal of Physical Oceanography, 50, 2507-2527, 2020.
- 1077 Hasle, G. R., and Syvertsen, E. E.: Marine diatoms, Identifying marine phytoplankton.
- 1078 Academic Press, San Diego, CA, 5–385, 1997.





- 1079 Hayashida, H., Matear, R. J., and Strutton, P. G.: Background nutrient concentration
- determines phytoplankton bloom response to marine heatwaves, Global Change Biology,
- 1081 26, 4800-4811, https://doi.org/10.1111/gcb.15255, 2020.
- He, Q., Zhan, W., Feng, M., Gong, Y., Cai, S., and Zhan, H.: Common occurrences of
- 1083 subsurface heatwaves and cold spells in ocean eddies, Nature, 1-7, 2024.
- 1084 Hobday, A. J., Alexander, L. V., Perkins, S. E., Smale, D. A., Straub, S. C., Oliver, E. C.,
- 1085 Benthuysen, J. A., Burrows, M. T., Donat, M. G., and Feng, M.: A hierarchical approach to
- defining marine heatwaves, Progress in oceanography, 141, 227-238, 2016.
- Hobday, A. J., Oliver, E. C., Gupta, A. S., Benthuysen, J. A., Burrows, M. T., Donat, M. G.,
- 1088 Holbrook, N. J., Moore, P. J., Thomsen, M. S., and Wernberg, T.: Categorizing and naming
- 1089 marine heatwaves, Oceanography, 31, 162-173, 2018.
- 1090 Hogg, A. M. C., Meredith, M. P., Blundell, J. R., and Wilson, C.: Eddy Heat Flux in the
- 1091 Southern Ocean: Response to Variable Wind Forcing, Journal of Climate, 21, 608-620,
- 1092 https://doi.org/10.1175/2007JCLI1925.1, 2008.
- 1093 Holbrook, N. J., Scannell, H. A., Sen Gupta, A., Benthuysen, J. A., Feng, M., Oliver, E. C. J.,
- 1094 Alexander, L. V., Burrows, M. T., Donat, M. G., Hobday, A. J., Moore, P. J., Perkins-
- 1095 Kirkpatrick, S. E., Smale, D. A., Straub, S. C., and Wernberg, T.: A global assessment of
- marine heatwaves and their drivers, Nature Communications, 10, 2624, 10.1038/s41467-
- 1097 019-10206-z, 2019.
- 1098 Holm-Hansen, O., Mitchell, B. G., Hewes, C. D., and Karl, D. M.: Phytoplankton blooms in
- the vicinity of Palmer Station, Antarctica, Polar Biol, 10, 49-57, 1989.
- 1100 Hutchins, D., Sedwick, P., DiTullio, G., Boyd, P., Queguiner, B., Griffiths, F., and Crossley,
- 1101 C.: Control of phytoplankton growth by iron and silicic acid availability in the subantarctic
- 1102 Southern Ocean: Experimental results from the SAZ Project, J. Geophys. Res, 106, 559-
- 1103 531, 2001.
- 1104 Hutchins, D. A., and Bruland, K. W.: Iron-limited diatom growth and Si:N uptake ratios in a
- 1105 coastal upwelling regime, Nature, 393, 561-564, 1998.
- 1106 Isla, E., Menschel, E., and González, H. H.: Intense autumnal coastal biogenic particle
- 1107 settling fluxes align with phytoplankton phenology changes off the western Antarctic
- 1108 Peninsula, Scientific Reports, 15, 10038, 10.1038/s41598-025-92914-9, 2025.
- 1109 Jabre, L., and Bertrand, E. M.: Interactive effects of iron and temperature on the growth of
- 1110 Fragilariopsis cylindrus, Limnology and Oceanography Letters, 5, 363-370, 2020.
- 1111 Johnsen, G., Dalløkken, R., Eikrem, W., Legrand, C., Aure, J., and Skjoldal, H. R.: ECO-
- 1112 PHYSIOLOGY, BIO-OPTICS AND TOXICITY OF THE ICHTHYOTOXIC CHRYSOCHROMULINA
- 1113 LEADBEATERI (PRYMNESIOPHYCEAE), Journal of Phycology, 35, 1465-1476,
- 1114 https://doi.org/10.1046/j.1529-8817.1999.3561465.x, 1999.
- Jones, M. E., Bromwich, D. H., Nicolas, J. P., Carrasco, J., Plavcová, E., Zou, X., and Wang,
- 1116 S.-H.: Sixty years of widespread warming in the southern middle and high latitudes (1957–
- 1117 2016), Journal of Climate, 32, 6875-6898, 2019.
- 1118 Kahru, M., Mitchell, B. G., Gille, S. T., Hewes, C. D., and Holm-Hansen, O.: Eddies enhance
- 1119 biological production in the Weddell-Scotia Confluence of the Southern Ocean,
- 1120 Geophysical Research Letters, 34, <a href="https://doi.org/10.1029/2007GL030430">https://doi.org/10.1029/2007GL030430</a>, 2007.
- 1121 Kang, J.-S., Kang, S.-H., Kim, D., and Kim, D.-Y.: Planktonic centric diatom Minidiscus
- 1122 chilensis dominated sediment trap material in eastern Bransfield Strait, Antarctica, Marine
- 1123 Ecology Progress Series, 255, 93-99, 2003.
- 1124 Kang, S.-H., and Fryxell, G. A.: Fragilariopsis cylindrus (Grunow) Krieger: The most
- abundant diatom in water column assemblages of Antarctic marginal ice-edge zones,
- 1126 Polar Biol, 12, 609-627, 10.1007/BF00236984, 1992.
- 1127 Kang, S. H., and Fryxell, G. A.: Phytoplankton in the Weddell Sea, Antarctica: composition,
- 1128 abundance and distribution in water-column assemblages of the marginal ice-edge zone
- 1129 during austral autumn, Marine Biology, 116, 335-348, 10.1007/BF00350024, 1993.





- 1130 Kang, S. H., and Lee, S. H.: Antarctic phytoplankton assemblage in the western Bransfield
- 1131 Strait region, February 1993: composition, biomass, and mesoscale distributions, Marine
- 1132 Ecology Progress Series, 129, 253-267, 1995.
- 1133 Karl, D. M., Tilbrook, B. D., and Tien, G.: Seasonal coupling of organic matter production
- 1134 and particle flux in the western Bransfield Strait, Antartica, Deep Sea Research Part A.
- 1135 Oceanographic Research Papers, 38, 1097-1126, https://doi.org/10.1016/0198-
- 1136 <u>0149(91)90098-Z</u>, 1991.
- 1137 Klunder, M. B., Laan, P., De Baar, H. J. W., Middag, R., Neven, I., and Van Ooijen, J.:
- 1138 Dissolved Fe across the Weddell Sea and Drake Passage: impact of DFe on nutrient
- 1139 uptake, Biogeosciences, 11, 651-669, 10.5194/bg-11-651-2014, 2014.
- 1140 Kopczyńska, E. E., and Ligowski, R.: Phytoplankton abundance and distribiution in the
- 1141 southern Drake Passage and the Bransfield Strait in February—March 1981 (BIOMASS-
- 1142 FIBEX), Polish Polar Research, 3, 193-202, 1982.
- 1143 Kuwata, A., and Takahashi, M.: Life-form population responses of a marine planktonic
- 1144 diatom, Chaetoceros pseudocurvisetus, to oligotrophication in regionally upwelled water,
- 1145 Marine Biology, 107, 503-512, 1990.
- 1146 Landry, M. R., Selph, K. E., Brown, S. L., Abbott, M. R., Measures, C. I., Vink, S., Allen, C. B.,
- 1147 Calbet, A., Christensen, S., and Nolla, H.: Seasonal dynamics of phytoplankton in the
- 1148 Antarctic Polar Front region at 170° W, Deep Sea Research Part II: Topical Studies in
- 1149 Oceanography, 49, 1843-1865, 2002.
- 1150 Lange, C. B., Treppke, U. F., and Fischer, G.: Seasonal diatom fluxes in the Guinea Basin
- 1151 and their relationships to trade winds, hydrography and upwelling events, Deep Sea
- 1152 Research Part I: Oceanographic Research Papers, 41, 859-878, 1994.
- 1153 Latorre, M. P., Iachetti, C. M., Schloss, I. R., Antoni, J., Malits, A., de la Rosa, F., De Troch,
- 1154 M., Garcia, M. D., Flores-Melo, X., and Romero, S. I.: Summer heatwaves affect coastal
- 1155 Antarctic plankton metabolism and community structure, Journal of Experimental Marine
- 1156 Biology and Ecology, 567, 151926, 2023.
- 1157 Leblanc, K., Arístegui, J., Kopczynska, E., Marshall, H., Peloquin, J., Piontkovski, S.,
- 1158 Poulton, A., Quéguiner, B., Schiebel, R., and Shipe, R.: A global diatom database-
- abundance, biovolume and biomass in the world ocean, 2012.
- 1160 Leblanc, K., Quéguiner, B., Diaz, F., Cornet, V., Michel-Rodriguez, M., Durrieu de Madron,
- 1161 X., Bowler, C., Malviya, S., Thyssen, M., Grégori, G., Rembauville, M., Grosso, O., Poulain,
- 1162 J., de Vargas, C., Pujo-Pay, M., and Conan, P.: Nanoplanktonic diatoms are globally
- 1163 overlooked but play a role in spring blooms and carbon export, Nature Communications,
- 1164 9, 953, 10.1038/s41467-018-03376-9, 2018.
- 1165 Lee, H., Calvin, K., Dasgupta, D., Krinner, G., Mukherji, A., Thorne, P., Trisos, C., Romero, J.,
- 1166 Aldunce, P., and Barrett, K.: Climate change 2023: synthesis report. Contribution of
- 1167 working groups I, II and III to the sixth assessment report of the intergovernmental panel on
- 1168 climate change, 2023.
- 1169 Legendre, L., and Le Fèvre, J.: Microbial food webs and the export of biogenic carbon in
- 1170 oceans, Aquatic Microbial Ecology, 9, 69-77, 1995.
- 1171 Leventer, A.: Sediment trap diatom assemblages from the northern Antarctic Peninsula
- 1172 region, Deep Sea Research Part A. Oceanographic Research Papers, 38, 1127-1143,
- 1173 <u>http://dx.doi.org/10.1016/0198-0149(91)90099-2</u>, 1991a.
- 1174 Leventer, A.: Sediment trap diatom assemblages from the northern Antarctic Peninsula
- 1175 region, Deep Sea Research Part A. Oceanographic Research Papers, 38, 1127-1143,
- 1176 https://doi.org/10.1016/0198-0149(91)90099-2, 1991b.
- 1177 Leventer, A.: Modern distribution of diatoms in sediments from the George V Coast,
- 1178 Antarctica, Marine Micropaleontology, 19, 315-332, 1992.
- 1179 Liebezeit, G.: Particulate carbohydrate fluxes in the Bransfield Strait and the Drake
- 1180 Passage, Marine Chemistry, 20, 255-264, 1987.





- 1181 Lundholm, N., and Hasle, G. R.: Are Fragilariopsis cylindrus and Fragilariopsis nana
- 1182 bipolar diatoms?–Morphological and molecular analyses of two sympatric species, Nova
- 1183 Hedwigia, Beiheft, 133, 231-250, 2008.
- 1184 Majewska, R., Kuklinski, P., Balazy, P., Yokoya, N. S., Paternostro Martins, A., and De
- 1185 Stefano, M.: A comparison of epiphytic diatom communities on Plocamium cartilagineum
- 1186 (Plocamiales, Florideophyceae) from two Antarctic areas, Polar Biol, 38, 189-205,
- 1187 10.1007/s00300-014-1578-7, 2015.
- 1188 Malinverno, E., Triantaphyllou, M. V., and Dimiza, M. D.: Coccolithophore assemblage
- 1189 distribution along a temperate to polar gradient in the West Pacific sector of the Southern
- 1190 Ocean (January 2005), Micropaleontology, 61, 489–506, 2015.
- 1191 Martin, J. H., Fitzwater, S. E., and Gordon, R. M.: Iron deficiency limits phytoplankton
- 1192 growth in Antarctic waters, Global Biogeochemical Cycles, 4, 5-12,
- 1193 doi:10.1029/GB004i001p00005, 1990.
- 1194 Martínez, J., Leonelli, F. E., García-Ladona, E., Garrabou, J., Kersting, D. K., Bensoussan,
- 1195 N., and Pisano, A.: Evolution of marine heatwaves in warming seas: the Mediterranean Sea
- 1196 case study, Frontiers in Marine Science, Volume 10 2023, 10.3389/fmars.2023.1193164,
- 1197 2023.
- 1198 Merchant, C. J., Embury, O., Bulgin, C. E., Block, T., Corlett, G. K., Fiedler, E., Good, S. A.,
- 1199 Mittaz, J., Rayner, N. A., and Berry, D.: Satellite-based time-series of sea-surface
- temperature since 1981 for climate applications, Scientific data, 6, 223, 2019.
- 1201 Meredith, M. P., and Hogg, A. M.: Circumpolar response of Southern Ocean eddy activity to
- 1202 a change in the Southern Annular Mode, Geophysical Research Letters, 33,
- 1203 https://doi.org/10.1029/2006GL026499, 2006.
- 1204 Meredith, M. P., Woodworth, P. L., Chereskin, T. K., Marshall, D. P., Allison, L. C., Bigg, G.
- 1205 R., Donohue, K., Heywood, K. J., Hughes, C. W., and Hibbert, A.: Sustained monitoring of
- 1206 the Southern Ocean at Drake Passage: Past achievements and future priorities, Reviews of
- 1207 Geophysics, 49, 2011.
- 1208 Meredith, M. P., Falk, U., Bers, A. V., Mackensen, A., Schloss, I. R., Ruiz Barlett, E., Jerosch,
- 1209 K., Silva Busso, A., and Abele, D.: Anatomy of a glacial meltwater discharge event in an
- 1210 Antarctic cove, Philosophical Transactions of the Royal Society A: Mathematical, Physical
- 1211 and Engineering Sciences, 376, 20170163, 2018.
- 1212 Moline, M. A., Claustre, H., Frazer, T. K., Schofield, O., and Vernet, M.: Alteration of the
- 1213 food web along the Antarctic Peninsula in response to a regional warming trend, Global
- 1214 Change Biology, 10, 1973-1980, 2004.
- Moline, M. A., Karnovsky, N. J., Brown, Z., Divoky, G. J., Frazer, T. K., Jacoby, C. A., Torres, J.
- 1216 J., and Fraser, W. R.: High latitude changes in ice dynamics and their impact on polar
- marine ecosystems, Annals of the New York Academy of Sciences, 1134, 267, 2008.
- 1218 Montes-Hugo, M., Vernet, M., Martinson, D., Smith, R., and Iannuzzi, R.: Variability on
- 1219 phytoplankton size structure in the western Antarctic Peninsula (1997–2006), Deep Sea
- 1220 Research Part II: Topical Studies in Oceanography, 55, 2106-2117, 2008.
- 1221 Montie, S., Thomsen, M. S., Rack, W., and Broady, P. A.: Extreme summer marine
- heatwaves increase chlorophyll a in the Southern Ocean, Antarctic Science, 32, 508-509,
- 1223 10.1017/S0954102020000401, 2020.
- 1224 Oh, J.-H., Noh, K. M., Lim, H.-G., Jin, E. K., Jun, S.-Y., and Kug, J.-S.: Antarctic meltwater-
- 1225 induced dynamical changes in phytoplankton in the Southern Ocean, Environmental
- 1226 Research Letters, 17, 024022, 10.1088/1748-9326/ac444e, 2022.
- 1227 Olguin, H. F., Boltovskoy, D., Lange, C. B., and Brandini, F.: Distribution of spring
- 1228 phytoplankton (mainly diatoms) in the upper 50 m of the Southwestern Atlantic Ocean
- 1229 (30-61 S), Journal of plankton research, 28, 1107-1128, 2006.
- 1230 Oliver, E. C., Donat, M. G., Burrows, M. T., Moore, P. J., Smale, D. A., Alexander, L. V.,
- 1231 Benthuysen, J. A., Feng, M., Sen Gupta, A., and Hobday, A. J.: Longer and more frequent
- marine heatwaves over the past century, Nature communications, 9, 1-12, 2018.





- 1233 Oliver, E. C. J., Benthuysen, J. A., Darmaraki, S., Donat, M. G., Hobday, A. J., Holbrook, N.
- 1234 J., Schlegel, R. W., and Sen Gupta, A.: Marine Heatwaves, Annual Review of Marine
- 1235 Science, 13, 313-342, https://doi.org/10.1146/annurev-marine-032720-095144, 2021.
- 1236 Orsi, A. H., Whitworth Iii, T., and Nowlin Jr, W. D.: On the meridional extent and fronts of
- 1237 the Antarctic Circumpolar Current, Deep Sea Research Part I: Oceanographic Research
- 1238 Papers, 42, 641-673, http://dx.doi.org/10.1016/0967-0637(95)00021-W, 1995.
- 1239 Patil, S. M., Mohan, R., Shetye, S. S., Gazi, S., Baumann, K.-H., and Jafar, S.: Biogeographic
- 1240 distribution of extant Coccolithophores in the Indian sector of the Southern Ocean, Marine
- 1241 Micropaleontology, 137, 16-30, https://doi.org/10.1016/j.marmicro.2017.08.002, 2017.
- 1242 Pauli, N.-C., Flintrop, C. M., Konrad, C., Pakhomov, E. A., Swoboda, S., Koch, F., Wang, X.-
- 1243 L., Zhang, J.-C., Brierley, A. S., Bernasconi, M., Meyer, B., and Iversen, M. H.: Krill and salp
- 1244 faecal pellets contribute equally to the carbon flux at the Antarctic Peninsula, Nature
- 1245 Communications, 12, 7168, 10.1038/s41467-021-27436-9, 2021.
- 1246 Peck, L. S., Barnes, D. K. A., Cook, A. J., Fleming, A. H., and Clarke, A.: Negative feedback
- 1247 in the cold: ice retreat produces new carbon sinks in Antarctica, Global Change Biology,
- 1248 16, 2614-2623, https://doi.org/10.1111/j.1365-2486.2009.02071.x, 2010.
- 1249 Peña, M. A., Nemcek, N., and Robert, M.: Phytoplankton responses to the 2014–2016
- 1250 warming anomaly in the northeast subarctic Pacific Ocean, Limnology and Oceanography,
- 1251 64, 515-525, <a href="https://doi.org/10.1002/lno.11056">https://doi.org/10.1002/lno.11056</a>, 2019.
- 1252 Plum, C., Hillebrand, H., and Moorthi, S.: Krill vs salps: dominance shift from krill to salps
- is associated with higher dissolved N:P ratios, Scientific Reports, 10, 5911,
- 1254 10.1038/s41598-020-62829-8, 2020.
- 1255 Rigual-Hernández, A. S., Trull, T. W., Bray, S. G., Closset, I., and Armand, L. K.: Seasonal
- 1256 dynamics in diatom and particulate export fluxes to the deep sea in the Australian sector
- of the southern Antarctic Zone, Journal of Marine Systems, 142, 62-74,
- 1258 <a href="http://dx.doi.org/10.1016/j.jmarsys.2014.10.002">http://dx.doi.org/10.1016/j.jmarsys.2014.10.002</a>, 2015.
- 1259 Rigual-Hernández, A. S., Trull, T. W., Bray, S. G., and Armand, L. K.: The fate of diatom
- 1260 valves in the Subantarctic and Polar Frontal Zones of the Southern Ocean: Sediment trap
- 1261 versus surface sediment assemblages, Palaeogeography, Palaeoclimatology,
- 1262 Palaeoecology, 457, 129-143, http://dx.doi.org/10.1016/j.palaeo.2016.06.004, 2016.
- 1263 Rigual-Hernández, A. S., Trull, T. W., Flores, J. A., Nodder, S. D., Eriksen, R., Davies, D. M.,
- 1264 Hallegraeff, G. M., Sierro, F. J., Patil, S. M., Cortina, A., Ballegeer, A. M., Northcote, L. C.,
- 1265 Abrantes, F., and Rufino, M. M.: Full annual monitoring of Subantarctic Emiliania huxleyi
- 1266 populations reveals highly calcified morphotypes in high-CO2 winter conditions, Scientific
- 1267 Reports, 10, 2594, 10.1038/s41598-020-59375-8, 2020a.
- 1268 Rigual-Hernández, A. S., Trull, T. W., Nodder, S. D., Flores, J. A., Bostock, H., Abrantes, F.,
- 1269 Eriksen, R. S., Sierro, F. J., Davies, D. M., Ballegeer, A. M., Fuertes, M. A., and Northcote, L.
- 1270 C.: Coccolithophore biodiversity controls carbonate export in the Southern Ocean,
- 1271 Biogeosciences, 17, 245-263, 10.5194/bg-17-245-2020, 2020b.
- 1272 Rigual Hernández, A. S., Flores, J. A., Sierro, F. J., Fuertes, M. A., Cros, L., and Trull, T. W.:
- 1273 Coccolithophore populations and their contribution to carbonate export during an annual
- 1274 cycle in the Australian sector of the Antarctic zone, Biogeosciences, 15, 1843-1862,
- 1275 10.5194/bg-15-1843-2018, 2018.
- 1276 Rintoul, S. R., Donguy, J. R., and Roemmich, D. H.: Seasonal evolution of upper ocean
- 1277 thermal structure between Tasmania and Antarctica, Deep Sea Research Part I:
- 1278 Oceanographic Research Papers, 44, 1185-1202, http://dx.doi.org/10.1016/S0967-
- 1279 <u>0637(96)00125-2</u>, 1997.
- 1280 Rintoul, S. R., and Sokolov, S.: Baroclinic transport variability of the Antarctic Circumpolar
- 1281 Current south of Australia, J. Geophys. Res, 106, 2815-2832, 2001.
- 1282 Rintoul, S. R., Chown, S. L., DeConto, R. M., England, M. H., Fricker, H. A., Masson-
- 1283 Delmotte, V., Naish, T. R., Siegert, M. J., and Xavier, J. C.: Choosing the future of Antarctica,
- 1284 Nature, 558, 233-241, 10.1038/s41586-018-0173-4, 2018.





- 1285 Rivero-Calle, S., Gnanadesikan, A., Del Castillo, C. E., Balch, W. M., and Guikema, S. D.:
- 1286 Multidecadal increase in North Atlantic coccolithophores and the potential role of rising
- 1287 CO2, Science, 350, 1533-1537, 10.1126/science.aaa8026, 2015.
- 1288 Saavedra-Pellitero, M., and Baumann, K.-H.: Comparison of living and surface sediment
- 1289 coccolithophore assemblages in the Pacific sector of the Southern Ocean,
- 1290 Micropaleontology, 61, 507-520, 2015.
- 1291 Saavedra-Pellitero, M., Baumann, K. H., Fuertes, M. Á., Schulz, H., Marcon, Y., Vollmar, N.
- 1292 M., Flores, J. A., and Lamy, F.: Calcification and latitudinal distribution of extant
- 1293 coccolithophores across the Drake Passage during late austral summer 2016,
- 1294 Biogeosciences, 16, 3679-3702, 10.5194/bg-16-3679-2019, 2019.
- 1295 Schlitzer, R.: Ocean Data View, <a href="https://odv.awi.de">https://odv.awi.de</a>, 2021.
- 1296 Scott, F. J., and Marchant, H. J.: Antarctic marine protists, 2005.
- 1297 Servettaz, A. P. M., Isaji, Y., Yoshikawa, C., Jang, Y., Khim, B. K., Ryu, Y., Sigman, D. M.,
- 1298 Ogawa, N. O., Jiménez-Espejo, F. J., and Ohkouchi, N.: Sea ice and mixed layer depth
- 1299 influence on nitrate depletion and associated isotopic effects in the Drake Passage-
- 1300 Weddell Sea region, Southern Ocean, Biogeosciences, 22, 2239-2260, 10.5194/bg-22-
- 1301 2239-2025, 2025.
- 1302 Silva, J. F. d., Oliveira, M. A., Paidano Alves, R., Vestena Cassol, A. P., Ribeiro da
- 1303 Anunciação, R., Pereira da Silva, E., Schünemann, A. L., and Batista Pereira, A.:
- 1304 Geographic distribution of epilithic diatoms (Bacillariophyceae) in Antarctic lakes,
- 1305 South Shetland Islands, Maritime Antarctica Region, Check List, 15, 797-809, 2019.
- 1306 Smetacek, V., Assmy, P., and Henjes, J.: The role of grazing in structuring Southern Ocean
- 1307 pelagic ecosystems and biogeochemical cycles, Antarctic Science, 16, 541-558,
- 1308 doi:10.1017/S0954102004002317, 2004.
- 1309 Smith Jr., W. O., and Gordon, L. I.: Hyperproductivity of the Ross Sea (Antarctica) polynya
- 1310 during austral spring, Geophysical Research Letters, 24, 233-236,
- 1311 https://doi.org/10.1029/96GL03926, 1997.
- 1312 Smith, K. E., Burrows, M. T., Hobday, A. J., King, N. G., Moore, P. J., Sen Gupta, A.,
- 1313 Thomsen, M. S., Wernberg, T., and Smale, D. A.: Biological impacts of marine heatwaves,
- 1314 Annual review of marine science, 15, 119-145, 2023.
- 1315 Suryawanshi, K., Jena, B., Bajish, C., and Anilkumar, N.: Recent decline in Antarctic sea
- 1316 ice cover from 2016 to 2022: insights from satellite observations, argo floats, and model
- 1317 reanalysis, Tellus A: Dynamic Meteorology and Oceanography, 75, 2023.
- 1318 Tagliabue, A., Sallee, J.-B., Bowie, A. R., Levy, M., Swart, S., and Boyd, P. W.: Surface-water
- iron supplies in the Southern Ocean sustained by deep winter mixing, Nature Geosci, 7,
- 1320 314-320, 10.1038/ngeo2101
- 1321 http://www.nature.com/ngeo/journal/v7/n4/abs/ngeo2101.html#supplementary-
- 1322 <u>information</u>, 2014.
- 1323 Takeda, S.: Influence of iron availability on nutrient consumption ratio of diatoms in
- 1324 oceanic waters, Nature, 393, 774-777, 1998.
- 1325 Tetzner, D., Thomas, E., and Allen, C.: A validation of ERA5 reanalysis data in the Southern
- 1326 Antarctic Peninsula—Ellsworth land region, and its implications for ice core studies,
- 1327 Geosciences, 9, 289, 2019.
- 1328 Thomalla, S. J., Nicholson, S.-A., Ryan-Keogh, T. J., and Smith, M. E.: Widespread changes
- 1329 in Southern Ocean phytoplankton blooms linked to climate drivers, Nature Climate
- 1330 Change, 13, 975-984, 10.1038/s41558-023-01768-4, 2023.
- 1331 Toggweiler, J., and Samuels, B.: Effect of Drake Passage on the global thermohaline
- 1332 circulation, Deep Sea Research Part I: Oceanographic Research Papers, 42, 477-500,
- 1333 1995.





- 1334 Treppke, U. F., Lange, C. B., and Wefer, G.: Vertical fuxes of diatoms and silicofagellates in
- 1335 the eastern equatorial Atlantic, and their contribution to the sedimentary record, Marine
- 1336 Micropaleontology, 28, 73-96, 1996.
- 1337 Trull, T. W., Passmore, A., Davies, D. M., Smit, T., Berry, K., and Tilbrook, B.: Distribution of
- 1338 planktonic biogenic carbonate organisms in the Southern Ocean south of Australia: a
- baseline for ocean acidification impact assessment, Biogeosciences, 15, 31-49, 2018.
- 1340 Turner, J., Lu, H., King, J., Marshall, G. J., Phillips, T., Bannister, D., and Colwell, S.: Extreme
- temperatures in the Antarctic, Journal of Climate, 34, 2653-2668, 2021.
- 1342 Vaughan, D. G., Marshall, G. J., Connolley, W. M., Parkinson, C., Mulvaney, R., Hodgson, D.
- 1343 A., King, J. C., Pudsey, C. J., and Turner, J.: Recent Rapid Regional Climate Warming on the
- 1344 Antarctic Peninsula, Climatic Change, 60, 243-274, 10.1023/A:1026021217991, 2003.
- 1345 Venables, H., and Moore, C. M.: Phytoplankton and light limitation in the Southern Ocean:
- 1346 Learning from high-nutrient, high-chlorophyll areas, Journal of Geophysical Research:
- 1347 Oceans, 115, C02015, 10.1029/2009JC005361, 2010.
- 1348 Vernet, M., Smith Jr, K. L., Cefarelli, A. O., Helly, J. J., Kaufmann, R. S., Lin, H., Long, D. G.,
- 1349 Murray, A. E., Robison, B. H., and Ruhl, H. A.: Islands of ice: Influence of free-drifting
- 1350 Antarctic icebergs on pelagic marine ecosystems, Oceanography, 25, 2012.
- 1351 Villafañe, V. E., Helbling, E. W., and Holm-Hansen, O.: Spatial and temporal variability of
- 1352 phytoplankton biomass and taxonomic composition around Elephant Island, Antarctica,
- during the summers of 1990–1993, Marine Biology, 123, 677-686, 10.1007/bf00349110,
- 1354 1995.
- 1355 Wernberg, T., Smale, D. A., Tuya, F., Thomsen, M. S., Langlois, T. J., de Bettignies, T.,
- 1356 Bennett, S., and Rousseaux, C. S.: An extreme climatic event alters marine ecosystem
- 1357 structure in a global biodiversity hotspot, Nature Climate Change, 3, 78-82,
- 1358 10.1038/nclimate1627, 2013.
- 1359 Wernberg, T., Bennett, S., Babcock, R. C., de Bettignies, T., Cure, K., Depczynski, M.,
- 1360 Dufois, F., Fromont, J., Fulton, C. J., Hovey, R. K., Harvey, E. S., Holmes, T. H., Kendrick, G.
- 1361 A., Radford, B., Santana-Garcon, J., Saunders, B. J., Smale, D. A., Thomsen, M. S., Tuckett,
- 1362 C. A., Tuya, F., Vanderklift, M. A., and Wilson, S.: Climate-driven regime shift of a
- temperate marine ecosystem, Science, 353, 169-172, doi:10.1126/science.aad8745,
- 1364 2016.
- 1365 Wilks, J. V., Nodder, S. D., and Rigual-Hernández, A.: Diatom and coccolithophore species
- 1366 fluxes in the Subtropical Frontal Zone, east of New Zealand, Deep Sea Research Part I:
- 1367 Oceanographic Research Papers, 169, 103455, https://doi.org/10.1016/j.dsr.2020.103455,
- 1368 2021.
- 1369 Wright, S. W., van den Enden, R. L., Pearce, I., Davidson, A. T., Scott, F. J., and Westwood,
- 1370 K. J.: Phytoplankton community structure and stocks in the Southern Ocean (30–80 E)
- determined by CHEMTAX analysis of HPLC pigment signatures, Deep Sea Research Part II:
- 1372 Topical Studies in Oceanography, 57, 758-778, 2010.
- 1373 Young, J., Geisen, M., Cross, L., Kleijne, A., Sprengel, C., Probert, I., and Østergaard, J.: A
- 1374 guide to extant coccolithophore taxonomy, Journal of Nanoplankton Research Special
- 1375 Issue 1, International Nannoplankton Association, 2003.
- 1376 Nannotax3 website: http://www.mikrotax.org/Nannotax3 access: July 2021, 2024.
- 1377 Zhu, J., Xie, A., Qin, X., Wang, Y., Xu, B., and Wang, Y.: An assessment of ERA5 reanalysis
- 1378 for Antarctic near-surface air temperature, Atmosphere, 12, 217, 2021.
- 1379 Zielinski, U., and Gersonde, R.: Diatom distribution in Southern Ocean surface sediments
- 1380 (Atlantic sector): Implications for paleoenvironmental reconstructions, Palaeogeography,
- 1381 Palaeoclimatology, Palaeoecology, 129, 213-250, http://dx.doi.org/10.1016/S0031-
- 1382 <u>0182(96)00130-7</u>, 1997.